KTH Chemical Science
and Engineering

Near field immobilization of selenium oxyanions

Anders Puranen

Doctoral thesis

School of Chemical Science and Engineering
Royal Institute of Technology
Stockholm 2010

ISBN 978-91-7415-819-9
ISSN 1654-1081
TRITA-CHE Report 2010:51

Printed by: Universitetsservice AB, Stockholm 2010

Abstract

The topic of this doctoral thesis is the potential near field immobilization of the radionuclide ^{79}Se after intrusion of groundwater into a spent nuclear fuel canister in a repository. ^{79}Se is a non naturally occurring long lived selenium isotope formed as a result of fission in nuclear fuel. Given the long half life (~3 x 10^5 y) and that the oxyanions of selenium are expected to be highly mobile and potentially difficult to immobilize the isotope is of interest for the long term safety assessment of high level waste repositories. In this work the near field has been limited to the study of processes at or near the UO_2 surface of (simulated) spent nuclear fuel and to processes occurring at or near the surface of iron (canister material) corroding under anoxic conditions.
Selenite ($HSeO_3^{2-}$) was found to adsorb onto palladium (simulated noble metal inclusion in spent nuclear fuel). Under hydrogen atmosphere selenite was reduced to elemental selenium with a rate constant of ~2 x 10^{-9} m s^{-1} (with respect to the Pd surface, 24 bar H_2) forming colloidal particles. The rate constant of selenite reduction was increased by about two orders of magnitude to ~2.5 x 10^{-7} m s^{-1} (with respect to the Pd surface, 10 bar H_2) for a UO_2 surface doped with Pd particles, indicating that UO_2 is an efficient co-catalyst to Pd. Selenate (SeO_4^{2-}) was neither adsorbed nor reduced in the presence of Pd, UO_2 and hydrogen. In the iron corrosion studies selenate was found to become reduced to predominantly elemental Se in the presence of a pristine iron surface. Iron covered by a corrosion layer of magnetite did however appear inert with respect to selenate whereas selenite was reduced. The reduction of dissolved uranyl into UO_2 by the corroding iron surfaces was found to significantly increase the removal rate of selenite as well as selenate. The uranyl was found to transiently transform the outer iron oxide layers on the iron, forming a reactive mixed Fe(II)/Fe(III) oxyhydroxide (Green rust). Exchanging the solution and increasing the carbonate content (from 2 mM to 20 mM $NaHCO_3$) only resulted in a minor, transient remobilization of uranium. Addition of H_2O_2 did however result in a significant release of uranium as well as selenium from the iron oxide surfaces. An irradiation experiment was also performed confirming the one electron reduction barrier of selenate as an important factor in systems where selenate reduction would be thermodynamically favorable.

Sammanfattning

Denna doktorsavhandling behandlar möjligheterna för reduktiv immobilisering av radionukliden ^{79}Se efter att grundvatten trängt in i en slutförvarskapsel i ett framtida slutförvar. ^{79}Se är en långlivad, icke naturligt förkommande, selenisotop som är en fissionsprodukt i utbränt kärnbränsle. Den långa halveringstiden (~3 x 10^5 år) och att selenoxidanjoner förväntas ha hög mobilitet samt vara svåra att immobilisera gör att isotopen är av vikt för säkerhetsanalyser för slutförvaring av utbränt kärnbränsle. Denna avhandling täcker möjliga immobiliseringsprocesser nära ytan av (simulerat) kärnbränsle samt processer i närvaro av järn (kapselmaterial) som korroderar under syrefria betingelser. Studierna visar att selenit ($HSeO_3^-$) adsorberas på ytan av palladium, Pd (Pd används som modellsubstans för de ädelmetallpartiklar som bildas i utbränt kärnbränsle). I närvaro av vätgas katalyserar Pd selenitreduktion under bildande av kolloidalt Se(0) med en hastighetskonstant av ~2 x 10^{-9} m s^{-1} (m.a.p Pd ytan, vid 24 bar H_2). Selenitreduktionshastigheteskonstanten ökade med ca två storleksordningar (~2,5 x 10^{-7} m s^{-1}, m.a.p Pd ytan, 10 bar H_2) för UO_2 som dopats med Pd vilket tyder på att UO_2 matrisen är aktiv i den katalytiska processen. Selenat (SeO_4^{2-}) tycks dock varken adsorberas eller reduceras under dessa betingelser. I närvaro av metalliskt järn reduceras selenat huvudsakligen till Se(0). Järn med ett yttre oxidlager av magnetit reducerade selenit men förfaller inert gentemot selenat. Reduktiv utfällning av uranyl ökar dock järn/järnoxidytornas förmåga att reducera såväl selenit som selenat. I samband med att den korroderande järnoxidytan reducerade uranyl bildades en transient Fe(II)/Fe(III) oxyhydroxid (grön rost). En ökning av lösningens karbonathalt (från 2 till 20 mM $NaHCO_3$) resulterade i en transient och ringa frisättning av uran. Tillsats av H_2O_2 orsakade dock en omfattande frisättning av uran samt selen från de korroderade järnytorna. Ett bestålningsexperiment utfördes även vilket bekräftade att selenat har en betydande en-elektronreduktionsbarriär som bör beaktas för system där selenatreduktion är termodynamiskt gynnsamt.

List of papers

I. A. Puranen, M. Trummer, M. Jonsson, *Can redox sensitive radionuclides be immobilized on the surface of spent nuclear fuel? – A model study on the reduction of Se (IV)$_{aq}$ on Pd-doped UO_2 under H_2 atmosphere,* Journal of Nuclear Materials, 392 (2009) 505-509

II. A. Puranen, M. Jansson, M. Jonsson, *A study on the immobilization of selenium oxyanions by H_2/Pd(s) in aqueous solution Confirmation of the one-electron reduction barrier of selenate,* Journal of Contaminant Hydrology, 111 (2010) 16-23

III. A. Puranen, M. Jonsson, R. Dähn, D. Cui, *Immobilization of selenate by iron in aqueous solution under anoxic conditions and the influence of uranyl,* Journal of Nuclear Materials, 392 (2009) 519-524

IV. A. Puranen, M. Jonsson, R. Dähn, D. Cui, *Reduction of selenite and selenate on anoxically corroded iron and the synergistic effect of uranyl reduction,* Journal of Nuclear Materials, 406 (2010), 230-237

V. A. Puranen, M. Jonsson, *Remobilization of U and Se reductively immobilized on iron oxide surfaces,* In manuscript.

Comments on my contribution to the papers

In paper **I**, I performed most of the experimental work and wrote a large part of the manuscript. For paper **II**, I performed all of the experimental work and prepared the major part of the manuscript. For papers **III** and **IV**, I performed most of the experimental work and most of the preparation of the manuscripts. For paper **V,** I performed all of the experimental work and prepared a minor part of the manuscript.

Papers not included in this thesis

K.O. Kvashnina, S.M. Butorin, D. Cui, J. Vegelius, A. Puranen, R. Gens, P. Glatzel, *Electron transfer during selenium reduction by iron surfaces in aqueous solution: high resolution X-ray absorption study*, J. Phys. Conf. Ser. (2009), 190, Institute of Physics Publishing

D. Cui, A. Puranen, J. Devoy, A. Scheidegger, O.X. Leupin, P. Wersin, R. Gens, K. Spahiu, *Reductive immobilization of ^{79}Se by iron canister under simulated repository environment*, J. Radioanal. Nucl. Chem. (2009), 282 349-354

J. A. Weitgenant, J. D. Mortison, D. J. O'Neill, B. Mowery, A. Puranen, P. Helquist*, *Samarium-Promoted Coupling of 1,10-Phenanthroline with Carbonyl Compounds for Synthesis of New Ligands*, J. Org. Chem., (2004) 69 2809-2815

Table of contents

Introduction

One of the largest, if not the largest, questions concerning the use of nuclear power is the controversial one of how to dispose of and guarantee the long term safety of the radioactive wastes, particularly the high level waste. In Sweden, the issue of the safe storage of nuclear waste in a way that does not burden coming generations is of such importance that it can, in fact, be said to be the largest current environmental protection project[1]. This thesis represents a very small part of this effort. The research in this field is often transnational with many countries sharing factors such as types of nuclear wastes, geological and to some degree also political constraints. Virtually all national research programs do however have the goal of disposing of the nuclear waste within the borders of the nation in which the waste was generated.

The proposed Swedish disposal concept for high level waste, the KBS-3, is depicted in Figure 1. It is designed to contain the spent nuclear fuel (SNF) for at least 100 000 years relying on four barriers. The outermost barrier is the granitic bedrock itself and the repository depth of about 500 m below the surface. The host rock should present a stable anoxic (oxygen free) environment for a very long timescale and contain few fractures to minimize the flow of groundwater. The rock also presents a large surface for the adsorption of escaping radionuclides. The next barrier is a compacted bentonite clay overpack about 35 cm thick. In contact with water the clay is expected to swell, filling small fractures in the rock preventing water from circulating, ideally limiting mass transport to and from the canister to diffusional processes. The migration of radionuclides would also be retarded by adsorption to the clay. The clay also provides shielding from rock movements. The SNF canister is the third barrier. It is composed of an outer corrosion resistant copper canister of 5 cm thickness, which is forseen to remain intact for the design life of the repository. A cast iron insert holding the spent nuclear fuel elements is placed in the copper canister prior to it being sealed by welding. The iron insert accounts for about half the weight of the complete canister (~25 metric tonnes in total) and provides mechanical strength for the canister. The forth and innermost barrier is the SNF itself. It is normally composed of ~95% UO_2 and ~5% fission products and higher actinides. Under the expected anoxic conditions the UO_2 matrix, which is a ceramic

[1] According to the 2009 annual report the Swedish Nuclear Waste Fund amounted to SEK 43 206 million at the end of 2009.

material, has very low solubility [1-3]. This low solubility constitutes the fourth barrier function once water has penetrated to the fuel surface.

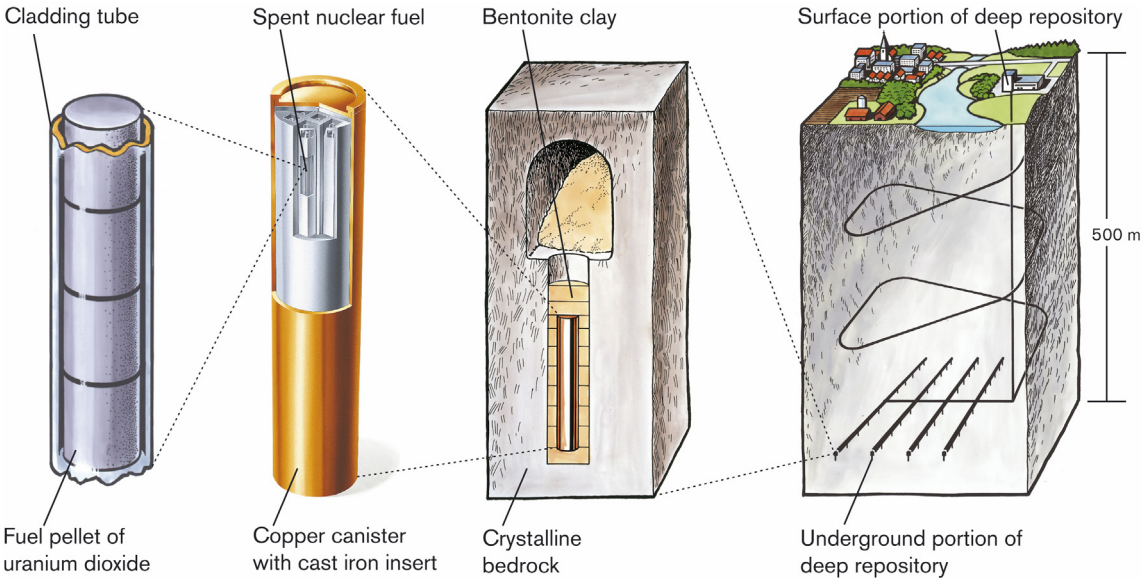

Figure 1: A schematic presentation of the KBS-3 concept for final disposal of spent nuclear fuel.

The dissolution of the spent nuclear fuel matrix in groundwater, liberating radioactive fission products and actinides is thus a key process. Even if the general environment is reducing the ionizing radiation emitted from the fuel will induce chemical processes in the water (radiolysis) close to the fuel surface producing both oxidants ($OH^{\cdot}$, H_2O_2, $HO_2^{\cdot}$ and O_2) and reductants (e_{aq}, $H^{\cdot}$ and H_2) [4]. The radiolytically produced oxidants will oxidize the UO_2, U(IV) to significantly more soluble uranyl, UO_2^{2+}, U(VI) and thereby enhance matrix dissolution [5]. It has been shown that the dominant oxidant with regard to the dissolution of UO_2 resulting from radiolysis in otherwise anoxic granitic groundwater is H_2O_2 [6]. The reactions involved in oxidative dissolution are shown in Reactions (1) and (2):

$$UO_{2(s)} + H_2O_2 \rightarrow UO_{2(s)}^{2+} + 2OH^- \quad (1)$$

$$UO_{2(s)}^{2+} \rightarrow UO_{2(aq)}^{2+} \quad (2)$$

Carbonate present as HCO_3^-, in the groundwater, increases the solubility of U(VI) and thereby the rate of oxidative fuel matrix dissolution even further [7-11]. The release of radionuclides from the SNF is thus strongly linked to the degree of oxidative dissolution of the UO_2-matrix. Another factor is the so called instant release fraction (IRF). The IRF

values are radionuclide and to some extent also fuel specific measures of the fraction of a radionuclide that is likely to be nearly instantaneously released from the fuel, for example from the grain boundaries or from the fuel-cladding gap, once the SNF comes in contact with water [12].

There are also processes that inhibit the release of radionuclides. The reductant hydrogen, H_2 which is radiolytically formed (as well as from the corrosion of iron) is of special importance. H_2 has been shown to have a considerable inhibiting effect on the dissolution of SNF [13-17]. Two major pathways for inhibition of oxidative dissolution of spent nuclear fuel have been identified, the competitive consumption of oxidants, and reduction of oxidized UO_2 on the SNF surface. These processes can be seen in reactions (3) and (4):

$$Ox + H_2 \rightarrow \mathrm{Re}\,d + 2H^+ \qquad (3)$$

$$UO_{2(s)}^{2+} + H_2 \rightarrow UO_{2(s)} + 2H^+ \qquad (4)$$

Both processes, (3) and (4) depend on catalytic noble metal particles composed of fission products (Pd, Mo, Ru, Tc, Rh and Te, often referred to as ε-particles) [18]. Reaction (4) has been shown to fully account for the observed decrease in UO_2 matrix dissolution and release of radionuclides in spent nuclear fuel leaching experiments under H_2 atmosphere [19]. The corrosion of iron could also have a very large impact on the release of radionuclides. Iron undergoing anaerobic corrosion produces magnetite and hydrogen gas (reaction 5) [20].

$$3Fe + 4H_2O \rightarrow Fe_3O_4 + 4H_2 \qquad (5)$$

This can lead to the build up of hydrogen pressures in the order of several MPa [21] in a breached SNF canister. The iron and iron corrosion products also have the potential to adsorb and also reductively immobilize escaping radionuclides or to consume oxidants such as H_2O_2.

This thesis deals with a particular radionuclide, ^{79}Se, a long lived β-decaying isotope that is formed by nuclear fission. Although ^{79}Se is a very minor radionuclide in spent nuclear fuel or other high level nuclear wastes it is considered of concern in the long term safety assessment of many high level waste repository concepts [22, 23]. This is due to the long half life and the potentially high mobility of the selenium oxyanions in various geological environments.

The topic of this thesis is to study the possible near field immobilization of Se released from SNF. In this case the simulated near field is considered as the inside of a breached SNF canister.

The scope can be divided into two parts. Firstly, to investigate if hydrogen in simulated anoxic groundwater reductively immobilizes selenium oxyanions in the presence of (simulated) SNF. Secondly, to investigate the reductive immobilization (or remobilization) of selenium oxyanions in contact with iron under simulated repository conditions. Since the bulk of the SNF is UO_2, the effects of solid UO_2 and dissolved uranyl on the immobilization of Se are also included in the studies. The methodology in the studies encompasses solution analysis and kinetic studies as well as characterization of surfaces and reaction products.

Selenium and the isotope ^{79}Se

In a geochemical context selenium may exist as the soluble selenium oxyanions, selenate, Se(VI) and selenite, Se(IV), as sparingly soluble Se(0) or as selenides Se(-II), Se(-I) that commonly form highly insoluble compunds such as FeSe. The environmental behavior of naturally occurring selenium is also of interest in a broader sense, not necessarily related to nuclear waste. Selenium is a vital trace element displaying high bioavailability and bioaccumulation potential (depending on its speciation) with importance in several physiological functions, such as the biosynthesis of coenzyme Q and glutathione peroxidase [24]. Its narrow tolerable range, possibly spanning as little as one order of magnitude between levels of selenium intake resulting in deficiency and those causing toxicity is rather unusual. Some areas are naturally Se deficient whereas other regions, such as the San Jouaqin valley in California suffer from excessive Se levels. Contamination of soils and waters from naturally occurring Se isotopes is thus of importance for man as well as livestock and wildlife in several parts of the world [25, 26]. Natural selenium contamination of waters can originate from seleniferrous soils and rock [27], mining [28], the refinement of metals or other industrial activities [29].

Even though a large number of studies have been performed concerning selenium in nuclear waste contexts there are still fundamental uncertainties concerning the ^{79}Se isotope itself. The half-life, $t_{1/2}$ of ^{79}Se is not firmly established as can be seen in Table 1 that summarizes the findings of various researchers. This is highly unusual given that the

half-life of nearly all isotopes of radiological importance are known down to an accuracy of 0.1 % or better [30].

Table 1: Published values for the half-life of ^{79}Se

Historical values		Half life [y]
1948	Glendenin [31]	$\geq 7 \times 10^6$
1949	Parker *et al* [32]	$\leq 6.5 \times 10^4$
Revised value		
1993	Singh *et al* [33]	$\leq 6.5 \times 10^5$
Calculated value		
2006	Zhou *et al* [34]	5.6×10^5
Measured values		
1995	Yu *et al* [35]	$4.8 \pm 0.4 \times 10^5$
1997	Jiang *et al* [36]	$1.1 \pm 0.2 \times 10^6$
2000	He *et al* [37]	$1.24 \pm 0.19 \times 10^5$
2002	Jiang *et al* [38]	$2.95 \pm 0.38 \times 10^5$
2002	He *et al* [39]	$2.80 \pm 0.36 \times 10^5$
2006	Bienvenu *et al* [40]	$3.77 \pm 0.19 \times 10^5$
2010	Jörg *et al* [41]	$3.27(8) \times 10^5$

The early value for the half life of ^{79}Se of $\leq 6.5 \times 10^4$ y from Parker *et al* [32] was and is still frequently cited despite the discovery of an error in the original paper that increased the upper estimated half life by a one order of magnitude to 6.5×10^5 y [33].

Later studies of the half life of ^{79}Se fall in the range of ~1-11 x 10^5 y. This rather large uncertainty is mainly due to difficulties in obtaining adequately pure ^{79}Se samples, since no established method for the production and purification of the isotope exists. ^{79}Se can currently only be obtained from spent nuclear fuel, in which it is a very minor component together with significantly larger amounts of other β-decaying fission products.

The amounts of ^{79}Se in spent nuclear fuel are largely based on calculated fission yields since the direct analysis of ^{79}Se has proven particularly difficult. The total fission yield of Se from ^{235}U is calculated to be ~0.5 % [42], of which ^{79}Se only comprises <10% of the total Se content [43], depending on the burn up of the fuel. For high burn up or MOX

fuels (Mixed oxide, containing both PuO_2 and UO_2), ^{239}Pu also contributes with a ^{79}Se fission yield that is slightly higher than of ^{235}U [43]. In fact, the total inventory of SNF from the operation of Swedish nuclear reactors, which has accumulated to about 5000 metric tonnes (late 2009), is roughly estimated to contain about 22.5 kg of the isotope ^{79}Se. A rather small amount, at least compared to other long lived potentially mobile radionuclides (the same calculation yields ~800 kg ^{129}I and ~3680 kg ^{99}Tc)[2].

To date there have mainly been two methods used to determine the actual ^{79}Se content of high level wastes, either by radiometric means or by ICP-MS. Detection of ^{79}Se by radiometric methods is difficult owing to the low β-energy (maximum energy 151 keV) and the absence of γ-emission (in addition to the uncertain half life). The considerably higher activities from comparatively short lived fission products such as ^{60}Co, ^{90}Sr and ^{137}Cs requires separation factors up to 10^6 which are hard to achieve while controlling the ^{79}Se content [44]. The contribution from ^{99}Tc, ^{147}Pm, ^{151}Sm, ^{93}Zr, or ^{241}Pu whose β-decay spectra are similar to that of ^{79}Se and are present at sometimes vastly greater amounts than that of ^{79}Se also complicates the analysis [44]. The use of ICP-MS generally requires less selective chemical separations than radiometric methods [45]. However, Se happens to be regarded as one of the more difficult elements to analyze by ICP-MS. This is due to the high ionization potential of Se (9.75 eV) which only causes ~30% of the Se to ionize in the Ar plasma, leading to poor sensitivity. For the direct measurement of ^{79}Se major isobaric interferences (near equal mass isotopes of different elements present in the sample) can be expected, in particular from ^{79}Br, which is also the β-decay product of ^{79}Se (nearly identical atomic weight) and which is an almost ever present minor contaminant from glass or the strong acids used to dissolve the nuclear materials.

Furthermore, since pure ^{79}Se cannot be obtained, it is necessary to use naturally occurring selenium isotopes for calibration. Since the exact isotopic Se composition of different spent nuclear fuels is not known (and varies to some degree as a function of burn up), indirect measurement based on other isotopes or isotope ratios is also precarious.

Given the considerable difficulties, data from determinations of ^{79}Se in high level wastes are very scarce, and generally presented as below the detection limit or without any attempt to compare the data with calculated inventory values [44, 45, 46, 47].

[2] Calculated using the CASMO inventory code at end of irradiation, assuming an average burnup of 35 MWd/kg U for a PWR fuel with an initial enrichment of 4% ^{235}U.

Since little is known about ^{79}Se in spent nuclear fuel, estimates of the chemical state and the distribution of ^{79}Se in the fuel largely depend on analogies with chemically similar elements and on the thermodynamic properties of Se.

There does not appear to be any explicit studies on the chemical state of Se in SNF. However based on its thermodynamic properties and comparing with the behavior of chemically similar tellurium, Te and neighboring elements, [48, 49] Se should either be in the oxide (+IV) or elemental (zero valent) state depending on the oxygen potential in the fuel. Assuming that Se is formed in its atomic form inside the UO_2-matrix as a result of actinide-fission, the distribution of the liberated oxygen atoms from the fission process is crucial to the speciation of the fission products, as well as the stochiometry and behavior of the fuel matrix. Given that oxidation of the inside of the cladding (under reactor operation) appears to be a sink of available oxygen, and that oxidation of the comparatively abundant fission product molybdenum, Mo should proceed prior to Se oxidation. Given that Mo is normally found to be at least partly in the metallic form it appears likely that Se should be in its reduced form in the fuel rather than as an oxide.

Due to the comparatively low melting and boiling points of expected Se species, such as elemental Se (mp: 221 °C, bp: 685 °C) or SeO_2 (bp 315 °C, sublimes), Se can be considered a volatile fission product during reactor operation. Se could thus be expected to segregate from the fuel matrix (UO_2) accumulating in pores or grain boundaries, in the so called rim zone of the fuel pellets or on surfaces in the gap space between the fuel and the cladding [12].

Looking at studies on Te, which could also be considered a volatile fission product and which is about five to ten times more abundant than Se (depending on fuel type and burn up), Te has been identified in the oxide form in the fuel clad gap for a variety of spent fuels such as LWR UO_2, and MOX or CANDU fuel [48, 50]. It should be noted that exposure to oxygen during sampling and handling of the fuel specimens could have an impact on the finding of tellurium oxides. Another source of Te that can also be suspected to hold a fraction of the Se inventory are the noble metal inclusions, also referred to as ε-particles. These are typically less than 1 μm large alloy particles commonly composed of the metals Mo, Ru, Tc, Pd, Rh and Te, also originating from the fission process. These noble metal inclusions are generally found in the grain boundaries [51]. Direct studies on the affinity of Se to become incorporated in these alloy particles in

nuclear fuel do not appear to exist, however a study on the fate of Se and Te in the high temperature processing of fission products from reprocessed nuclear waste found that Se did form a PdSe alloy [52]. If Ag can be considered a model for the nobel metal alloys the work of Kosec *et al* [53] show that both Se and Te forms a silver alloy in the temperature range expected in the nuclear fuel during reactor operation. Their work also supports the thermodynamic prediction that Te is oxidized first over Se. Since Te has been observed in noble metal particles it is thus possible that they also contain Se, albeit at a smaller fraction given the lower fission yield of Se.

Estimates of the instant release fraction, IRF puts the values for Se at ~1-20% of the inventory, [12, 54] (depending on burn up, and best or pessimistic estimation). Given that no Se has been reported for any of the numerous IRF and other SNF leaching studies performed to date it does however appear that the Se is largely retained in the SNF or remains immobilized in some other part of the system. It should be stressed that Se is a very minor fission product, the previously mentioned difficulties with detecting Se should also be kept in mind. Many SNF leaching experiments did not even include the possibility of detecting Se-isotopes by excluding mass numbers less than around 80-83 in the analysis (ICP-MS, presumably due to the mentioned isobaric interferences).

Interestingly the two billion years old natural reactor zones in Oklo, Gabon offers some natural analogues on the very long term stability of Se in nuclear fuels. Enriched levels of Se compared to the background of the area and roughly in agreement with a fissiogenic origin was found associated with the mineral uraninite in these ancient reactor cores [55], indicating that the Se had not migrated very far despite the considerable time scales. There is also evidence that Se may have been retained in the previously mentioned noble metal inclusion (also containing fissiogenic Te) that have been identified in the Oklo reactor zones [56].

Returning to the disposal of antropogenic nuclear waste. As mentioned, in order for the SNF to be able to release any radionuclides the canister must fail exposing the SNF to groundwater. From a thermodynamic viewpoint Se is expected to be in a reduced form once in contact with the groundwater (Eh -200 to -300 mV vs SHE, [57]), as can be seen in Figure 2. The pH is expected to be neutral to slightly alkaline (largely depending on the carbonate content of the groundwater) [57].

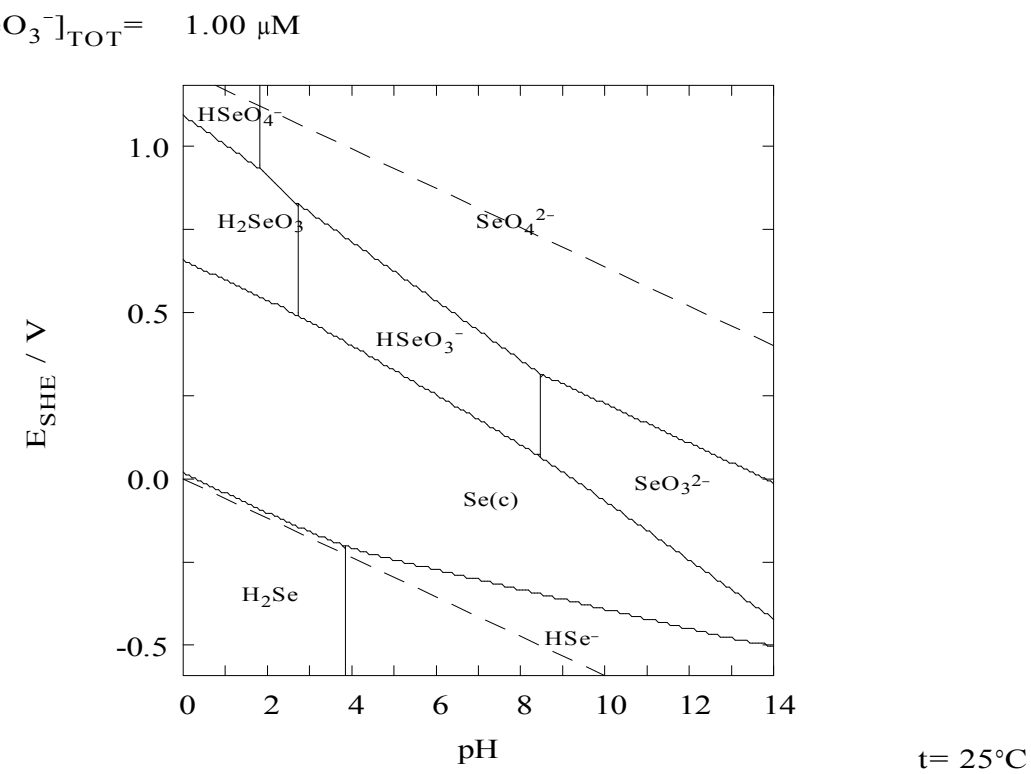

Figure 2: Predominance area of Se, calculated with MEDUSA using data from [64].

The mobility of Se under the reducing conditions should from a thermodynamic viewpoint be controlled by the Se(0)/HSe^- equilibrium and the solubility of various selenides. Particularly in the presence of iron or naturally occurring sulfides such as pyrite, FeS_2, forming selenides like FeSe and $FeSe_2$ with very low solubilities in the range of 10^{-10} M to 10^{-7} M [58, 59].

However if oxidative dissolution either by oxidizing radiolysis products such as H_2O_2 [6] formed by the inherent ionizing radiation of the SNF itself, or by transient penetration of oxygenated water (such as glacial melt water) is considered, released Se species should at least transiently be in an oxidized form, i.e. as the selenium oxyanions selenite or selenate. Under such conditions secondary uranyl minerals could also be present. Selenite (and to some degree selenate) could then be incorporated and immobilized by substituting silicate, phosphate or carbonate in these uranyl minerals [60]. Selenite also forms adsorption complexes on ferric oxides from the iron insert [61], whereas selenate is generally less readily adsorbed.

Many repository concepts incorporate some form of clay barrier around the SNF canisters, either by addition of a bentonite layer (KBS-3) or by positioning the repository

in a clay host rock. Under reducing conditions dissolved selenides could be strongly retarded in these barriers [62]. Whereas selenite and particularly selenate would likely be significantly more mobile [62, 63].

Although the fate of Se in the far field of a repository is outside the scope of this thesis it can be summarized in the following very simplified way. Adsorption of selenite on rock, soil and organic matter has been shown to decrease with increasing pH, selenate is generally less readily adsorbed and with less pH dependence. A simplified view is that whereas selenite is generally adsorbed via inner-sphere complexes (such as with organic matter and clays) selenate more commonly adsorbs via outer-sphere complexes, although evidence of selenate inner-sphere complexes also exists. These differences in sorption behavior is probably due to the electronic configuration of the selenite anion which forms a distorted pyramid with three bond pairs and one lone pair (with the lone pair promoting the formation of inner-sphere complexes). The selenate anion on the other hand is tetrahedral with four bond pairs and no lone pairs. There are also significant differences in acidity with selenious acid (H_2SeO_3) being a weaker acid with $pKa_1 \approx 2.70$ and $pKa_2 \approx 8.54$. Selenic acid (H_2SeO_4) is a considerably stronger acid with $pKa_1 \approx -2.01$ and $pKa_2 \approx 1.8$ [64]. Dissolved tetravalent selenium oxyanions would thus exist as a mixture of $HSeO_3^{2-}$ and SeO_3^{2-} anions at the expected neutral or slightly alkaline water of a bedrock repository, while hexavalent selenium would exist almost purely as SeO_4^{2-}.

The environmental selenium speciation, mobility and bioavailability also depend on biotic processes. Certain sulfur respiring bacteria can use selenium oxyanions as terminal electron acceptors, although sulfur independent Se respiring bacteria have also been identified, typically producing elemental Se. In large selenium chemistry resembles that of its group 16 neighbor sulfur. Se is thus known to form similar compounds to those of S, and to substitute S in a variety of minerals. For further information on the general bio and geochemistry of selenium the reader is referenced to two recent review papers [25, 26].

Experimental details

Paper I

The palladium doped uranium dioxide pellets used in this study were hot pressed under vacuum from depleted UO_2 (Westinghouse Atom AB, ~16 μm particle size) and palladium powder (Aldrich, 99.9+ % Pd, average particle size 1–1.5 μm) yielding pellets of 13 mm diameter and 2.6 mm thickness with a geometric surface of ~372 mm^2. Details on the production of the pellets are given in [65]. Prior to the experiments the pellets were cleaned by ultrasonication for 30 s in a 20 mM $NaHCO_3$ solution, transferred to a glove box (nitrogen, <5 ppm O_2) and stored overnight in a fresh 20 mM $NaHCO_3$ solution. All experimental solutions were prepared inside the glove box from degassed Milli-Q deionized water (18 MΩ). The pellets were placed in glass vessels with their solutions and sealed in an autoclave that was transferred out of the glove box. The autoclave was purged with hydrogen and pressurized with H_2 to either 1 or 10 bar absolute pressure at room temperature. For sampling, the autoclave was transferred back into the glove box, and the Se(IV) concentration in the samples was measured by iodometry at 350 nm using a Jasco V-630 UV/VIS spectrophotometer. All samples were centrifuged (RCF 25 000g) prior to analysis.

Paper II

Palladium powder was supplied by Aldrich (99.9+% Pd, average particle size 1–1.5 μm) and was used as delivered. All solutions were prepared in a glove box (nitrogen, <1 ppm O_2) from deoxygenated Milli-Q water (18 MΩ). The adsorption experiments on Pd powder suspensions in the absence of H_2 were performed in the glove box in capped plastic bottles (40 ml solution) that were placed in a rocker. The glassware and plastic bottles used in the experiments were tested and were found not to adsorb any detectable quantity of selenium. The experiments with hydrogen were performed in a glass vessel (120 ml volume) placed in an autoclave equipped with a rotor made of PEEK (poly-ether-ether-ketone) and Teflon. The autoclave solutions were purged with nitrogen gas, followed by hydrogen purging prior to pressurization to 24 bar H_2. Liquid sampling was performed a few centimeters above the bottom of the vessel via PEEK tubing and a PEEK valve. The rotor was stopped 5 min prior to sampling to allow the Pd powder suspension to settle. The first volume corresponding to the volume of the sampling line

was discarded and the samples were immediately transferred to the glove box. A Jasco V-630 UV/VIS spectrophotometer was used to determine the selenite concentration in the samples by iodometry. Total Se was measured by ICP-OES. All samples were normally centrifuged (RCF 25000 g for 5 min) prior to analysis. For the irradiation experiments closed glass vessels purged with either argon or N_2O, filled with 10 ml 250 μM of either Na_2SeO_3 or Na_2SeO_4 and 10% 2-propanol or t-butanol was used. A 6 MeV Microtron (12.5 Hz, 4 μs pulse duration) electron accelerator irradiated the samples with an average dose rate of ~24 Gy/s (measured by Fricke dosimetry). The irradiation was performed at 1 min intervals with an intermittent cooling time of a few minutes, giving total irradiation times of ~6-15 min per sample. The samples were irradiated with a dose corresponding to three times the dose required to reduce the selenite or selenate in the samples to selenide, Se(−II). After irradiation, the solutions were extracted five times with dichloromethane to remove organic selenides before the aqueous phase was centrifuged and analyzed.

Paper III

Iron foils (Goodfellow 99.75%-Fe), 20 μm thick were cut inside a glove box (<0.1 ppm O_2), polished to expose a fresh surface and washed in distilled water to remove the polishing residues. The foils were divided into several small pieces with a total area ~4 cm^2 per sample. Plastic bottles with 50 ml solution were used. All solutions were prepared inside the glove box from degassed Milli-Q deionized water. The selenate used (Na_2SeO_4, Alfa Aesar, 99.8%) for the solutions was analyzed iodometrically to test for any selenite contamination, of which none could be detected. The selenium and uranium concentration in solutions was measured by ICP–OES.

Paper IV

The experimental procedure is largely similar to paper III. The polished iron foils were precorroded in a glass vessel which was filled with deoxygenated distilled water, sealed, thermally isolated and kept at 80 °C inside the glove box for 60 days. The foils were slightly bent to prevent them from laying flat on the bottom of the vessel. Iron powder (99.5% Fe, 140 μm diameter) kindly provided by Höganäs AB, was pre-corroded in the same manner as the iron foils. The redox potential of the experimental solutions was measured in the glove box using a Pt electrode and Metrohm Ag/AgCl reference electrode verified using saturated quinhydrone buffers at pH 4 and 7.

Instruments

- UV/Vis spectrophotometers: Jasco V-630 or WPA Lightwave S2000.
- ICP-OES: Varian Vista Ax or Thermo iCAP 6500
- Raman microscopes: Renishaw 1000, 633 nm HeNe Spectra Physics 127 laser. Renishaw inVia Reflex raman microscope with 532 nm laser.
- PCS: 90 Plus Particle Size Analyser, 488 nm 2 W Lexus Laser Model 95 Ion laser
- TEM: Philips Tecnai 10
- SEM: JEOL JSM 9460LV
- BET: Micromeritics Flowsorb II 2300 with 30 % N_2 in He
- Glove box: MBraun UNIlab, working gas N_2 or 0.003 % CO_2 in Ar. Typical O_2 level of <0.1 ppm measured.
- XAS: μ-XAS beamline at SLS [66]

Analytical methods

Solution analysis

A UV/VIS spectrophotometer was used to determine the selenite concentration in the samples by iodometry with all preparations performed in the anaerobic glove box. The iodometry (outlined in reactions 6 and 7) is based on the reduction of selenite by an excess of iodide in HCl (pH ~1) yielding triiodide which was monitored spectrophotometrically at 350 nm.

$$H_2SeO_3 + 4I^- + 4H^+ \rightarrow Se + 2I_2 + 3H_2O \quad (6)$$

$$I_2 + I^- \rightarrow I_3^- \quad (7)$$

Total Se was measured by ICP-OES. All samples were normally centrifuged (RCF 25 000 g for 5 minutes) prior to analysis.

Raman microscopy

Samples were dried and sealed by kapton tape under a cover glass and transferred out of the glove box for investigation by Raman microscopy. Either a Renishaw 1000 system with a 633 nm Spectra Physics model 127 laser or a Renishaw inVia Reflex raman microscope with a 532 nm laser was used. The spectra were recorded at room temperature using 20x and 80x magnification, corresponding to a spatial resolution of 5 μm or less. In order avoid sample degradation the light was filtered down to a spot intensity of ~0.5 mW or less. Cosmic ray suppression was employed.

X-ray spectroscopy

Micro-XAS spectroscopy and fluorescence microprobe mapping was performed at the microXAS beamline at the Swiss Light Source (SLS) [66]. The beam size was ~2x6 μm^2. Commercial liquid sodiumselenate, selenite, solid gray elemental Se, ferroselite and dioctyldiselenide were used as Se references. The dioctyldiselenide, Se(-I) reference prepared according to Syper et al. [67] and confirmed by NMR was kindly provided by Prof. Lars Engman at Uppsala University, Sweden. For uranium uranylnitrate and UO_2 references were used. Prior to transport to the beamline the samples were sealed (in the glovebox) in a double air tight container with freshly regenerated oxygen scavenging copper pellets in the outer compartment of the container. The colour of the copper pellets indicated no intrusion of oxygen prior to the XAS-analysis. Multiple μ-XANES spectra were recorded for each region of interest and the first and last of each series was compared to check for possible redox reactions induced by the high photon flux of the synchrotron beam, of which no indication was found. The U or Se in the dried and encapsulated samples did not appear to be sensitive to oxidation by air or by redox effects while being handled at the beamline over the course of a few days and repeated beam exposures. Data averaging (three to five spectra from each spot), background correction and normalization was performed in the program WINXAS [68]. All spectra were collected at room temperature.

Results and discussion

Selenium immobilization on the surface of simulated spent nuclear fuel under hydrogen atmosphere (Paper I-II).

A number of studies have shown that the noble metal particles (alloys of Pd, Mo, Ru, Tc, Rh, Te, often referred to as ε-particles) in SNF play a major role in catalyzing H_2 reduction of the oxidized UO_2 fuel matrix [19, 69]. Thus it is possible that these particles also could have a major impact on the state of other redox sensitive radionuclides (such as the long lived fission product ^{79}Se) present in spent nuclear fuel. In fact Cui et al [70] recently published evidence for partial immobilization of selenite under hydrogen conditions in the presence of noble metal particles extracted from SNF. In our studies fine grained (~1.25 μm diameter) metallic Pd powder serves as a model for the noble metal alloys in SNF. In order to simulate groundwater the solution was composed of 10 mM NaCl and 10 mM $NaHCO_3$. The solution also buffers the pH at ~8.3 and maintains almost constant ionic strength in the experiments. As can be seen in Figure 3 selenite was found to adsorb on the Pd powder (in the absence of hydrogen). Lowering the pH (in the absence of carbonate, pH adjusted by addition of HCl) was found to dramatically enhance the degree of adsorption (not shown). Interestingly, no selenate adsorption on the Pd powder was observed at pH 1 (adjusted by HCl), in deionized water and at pH 8.3 (10 mM $NaHCO_3$), even when the Pd surface to volume ratio was increased beyond that in the selenite adsorption experiments (not shown).

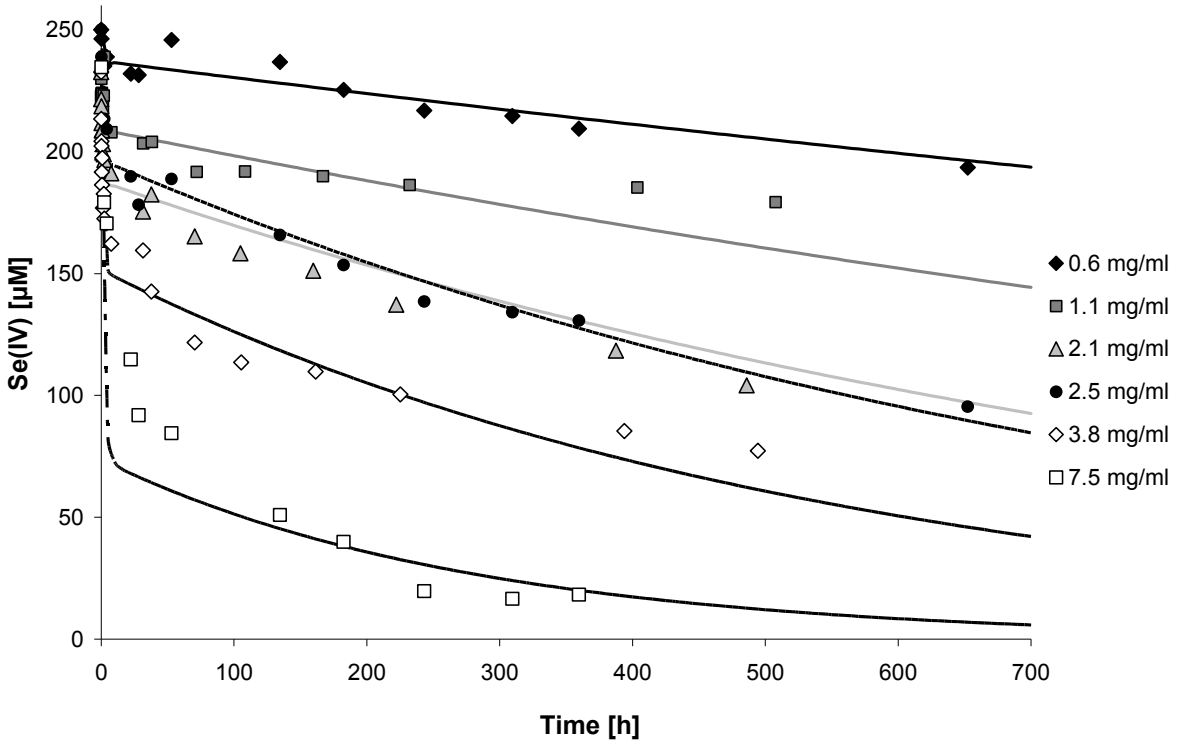

Figure 3: Se(IV) adsorption kinetics for Pd suspensions with varying Pd content (expressed in mg Pd/ml solution) in the absence of H_2 and results from the adsorption model (lines).

As can be seen in Figure 3 the initial rapid reduction in selenite concentration was followed by a significantly slower process. The cause of this is probably rapid formation of a selenite monolayer followed by slow multilayer sorption. The simplest way to describe the sorption dynamics is by simulation using two reactions, (8) and (9), where the second reaction accounts for the multilayer sorption.

$$Se(IV) + Pd \rightarrow Se_x\text{-}Pd \qquad (8)$$

$$Se(IV) + Se_x\text{-}Pd \rightarrow Se_{x+1}\text{-}Pd \qquad (9)$$

When the amount of selenite removed by the initial rapid adsorption is estimated for the various Pd surface to volume ratios (from Figure 3) and the measured BET surface area of 1.12 m^2/g for the Pd powder is used, an adsorption site density of approximately 10 selenite molecules per nm^2 is obtained. If this is assumed to correspond to a monolayer, the rather high site density indicates that a large fraction of the surface is active in the selenite adsorption. In reaction (9), Se_x-Pd (and Se_{x+1}-Pd) denotes Pd with multilayer sorption of selenite ($x \geq 1$). The number of available sites in a monolayer and the rate constants for the two sorption processes were fitted using the kinetic program package

Gepasi [71]. The fit was based on four of the data sets (excluding the highest and lowest Pd concentrations) and the resulting parameters were used to simulate all six data sets (represented as lines in Figure 3). As can be seen, this mechanistic approach reproduced the experimental observations fairly well.

In the presence of hydrogen, the initial rate of selenite removal appears to follow the proposed adsorption processes. However, beyond the initial adsorption the selenite concentration in solution decreased considerably faster when hydrogen was present (Figure 4).

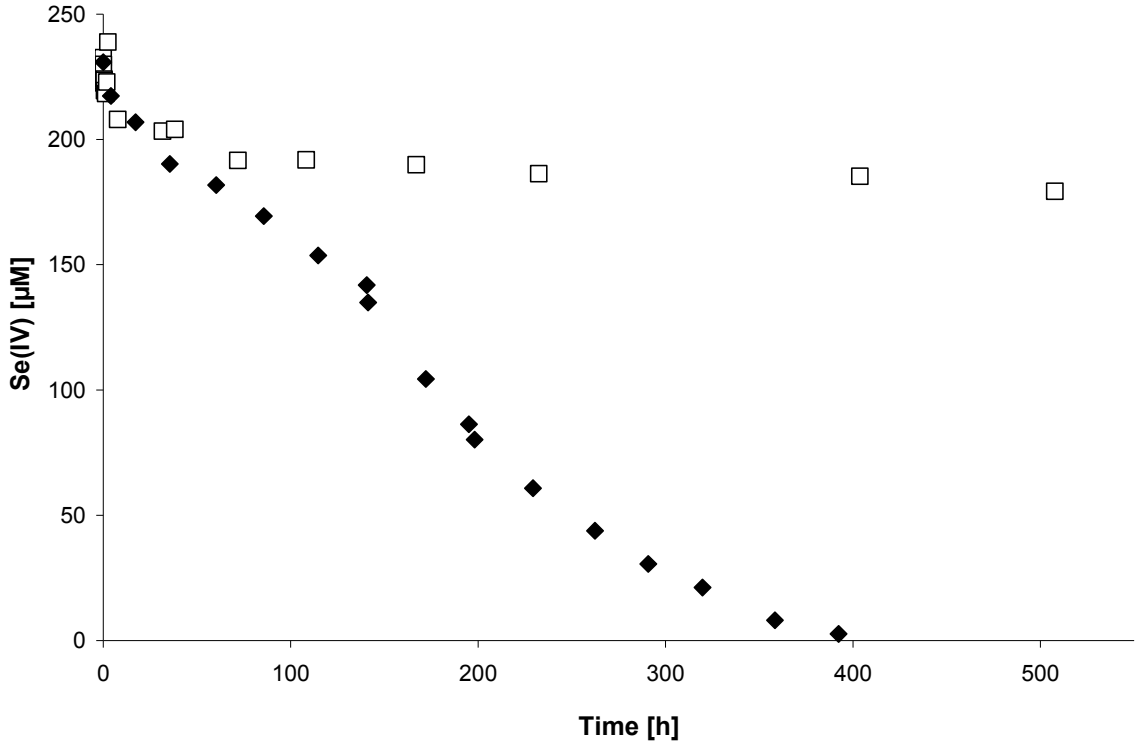

Figure 4: Se(IV) removal for similar S/V ratios of Pd with and without H_2. ♦: 1.25 mg Pd/ml, 24 bar H_2. □: 1.1 mg Pd/ml, no H_2.

As shown in Figure 5, in the presence of H_2, the aqueous Pd(s)/Se(IV) system displayed auto-catalytic behavior (i.e. the rate is increased with conversion).

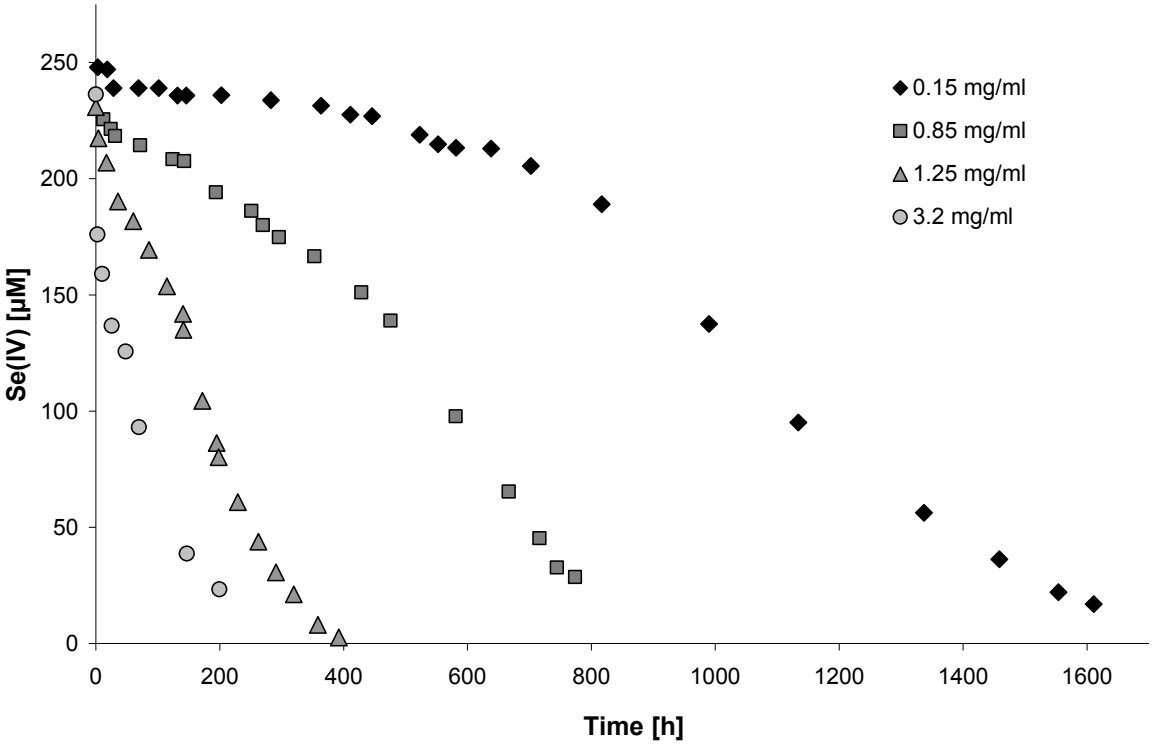

Figure 5: Se(IV) removal under 24 bar H_2 (10 mM NaCl, 10 mM $NaHCO_3$) with varying Pd S/V ratios.

The simplest way to describe the hydrogen induced reduction mechanism is by introducing two reactions where the first reaction accounted for reduction of selenite sorbed to Pd and the second reaction accounted for the observed auto-catalysis. At constant H_2 pressure, reactions (10) and (11) can be used for kinetic simulations.

$$Se_x\text{-Pd} \xrightarrow{H_2} Pd + Se(red) \qquad (10)$$

$$Se(IV) + Se(red) \xrightarrow{H_2} n\,Se(red) \qquad (11)$$

In the case where the Pd concentration was 0.85 mg/ml, the solution was replenished with more selenite after 800 hours. In Figure 6 the experimental data are fitted taking the sorption reactions (8 and 9) and reactions 10 and 11 into account.

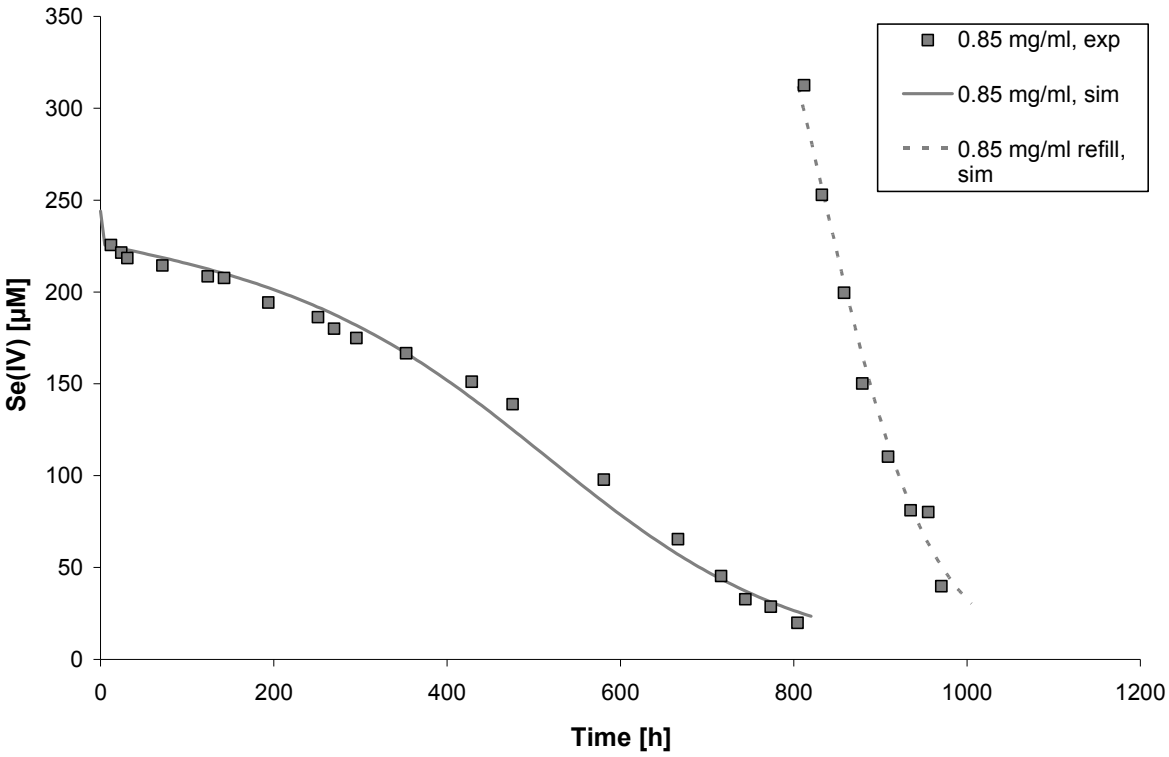

Figure 6: Comparison of kinetics under 24 bar H_2 (10 mM NaCl, 10 mM $NaHCO_3$) for 0.85 mg Pd /ml, including replenishment of Se(IV) at 800 h and the fitted simulation.

The fit was based on the first 800 hours and the obtained rate constants for reaction 10 and 11 were used to simulate the dynamics for the system replenished with more selenite. To maintain mass balance, *n* in reaction 11 should be 2. However, the replenished system could only be successfully simulated when $n > 2$. This implies that the auto-catalytic effect is not directly proportional to the amount of selenite reduced. It should also be noted that with this simple model it is not possible to fit all data sets with high accuracy using the same set of rate constants. The main reason for this is probably that heterogeneous auto-catalysis cannot be properly accounted for using homogeneous kinetics, as the catalytic activity of the solid product is expected to depend on particle size. Interestingly, elemental Se has been found to act as a co-catalyst to Pd in the reduction of aqueous oxygen [72], indicating that this may also be the case for the reduction of aqueous selenite. It is also possible that the selenite reduction proceeds all the way to selenide formation.

In addition, selenide can reduce selenite to elemental Se according to reaction 12 [73]:

$$6H^+ + 2Se^{2-} + SeO_3^{2-} \rightarrow 3Se + 3H_2O \qquad (12)$$

At the termination of the hydrogen experiments the autoclave was opened. The solutions commonly had a faint red/orange colour with some red precipitate. Upon exposure to air the red colour of the solutions as well as the amount of red precipitate increased over a few hours. The pH of the solutions also increased somewhat (from ~8.5 to ~9) during exposure to air. This can be interpreted as air-induced oxidation of selenide anions to elemental selenium (reaction 13).

$$H^+ + 2HSe^- + O_2 \rightarrow 2Se + H_2O + OH^- \qquad (13)$$

In some cases there was a faint unpleasant smell, indicating some degree of hydrogen selenide (H_2Se) formation, although the slightly alkaline pH of the solutions most certainly did not favor formation of gaseous hydrogen selenide.

Samples of the red precipitate that formed in the solutions under hydrogen atmosphere were analyzed by Raman spectroscopy (Figure 7). The strong band at 255 cm^{-1} is indicative of either amorphous or monoclinic elemental Se allotropes, which are commonly assigned positions at ~250-255 cm^{-1} [74, 75]. Due to the similar Raman spectra, differentiation between amorphous and monoclinic selenium was difficult. When the experimental solutions were left to age (capped at room temperature with a headspace of air), the red particles gradually transformed over the course of several weeks to a grey colour, identified by Raman analysis by its strong band at 236 cm^{-1} (Figure 7) as trigonal elemental selenium [74], which is thermodynamically the most stable elemental selenium allotrope [64].

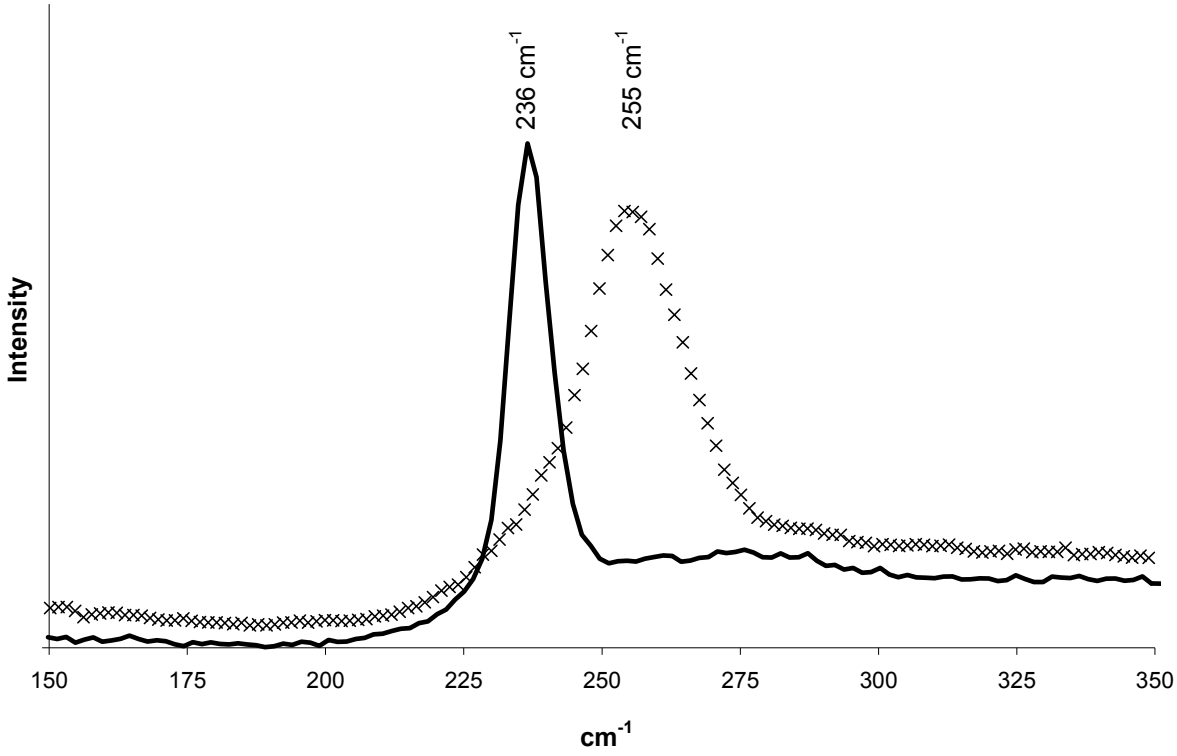

Figure 7: Raman spectra of the red precipitate directly from the autoclave (x) and air aged precipitate (line).

Since the reduction of selenite, at least partly, yields a colloidal product, the influence of the potential colloidal product on the method of analysis of selenite in solution was investigated for one of the experiments (1.25 mg Pd/ml, 24 bar H_2, Figure 8). The sampling procedure was the same as in the other Pd-powder autoclave experiments: the rotor was stopped for 5 minutes to allow heavier particles to settle, the first volume corresponding to the volume of the sampling tube was discarded and samples were collected and rapidly transferred to the glove box. In this case the samples were subjected to four different analytical steps: iodometric analysis, with and without prior centrifugation or ICP-OES analysis, with and without centrifugation. Assuming that any colloids are elemental Se with a density of ~4 g/cm^3 centrifugation at 25000 g for 5 minutes should precipitate all colloids larger than ~90 nm (according to Stokes law).

As can be seen in Figure 8, centrifugation did not appear to have a significant impact on the iodometric analysis, which is selenite-specific under the present conditions. This indicates that colloids if present in solution had a very limited impact on the measured selenite concentrations. It also tentatively indicates that colloids in solution do not contain a significant amount of adsorbed selenite available for iodometric analysis.

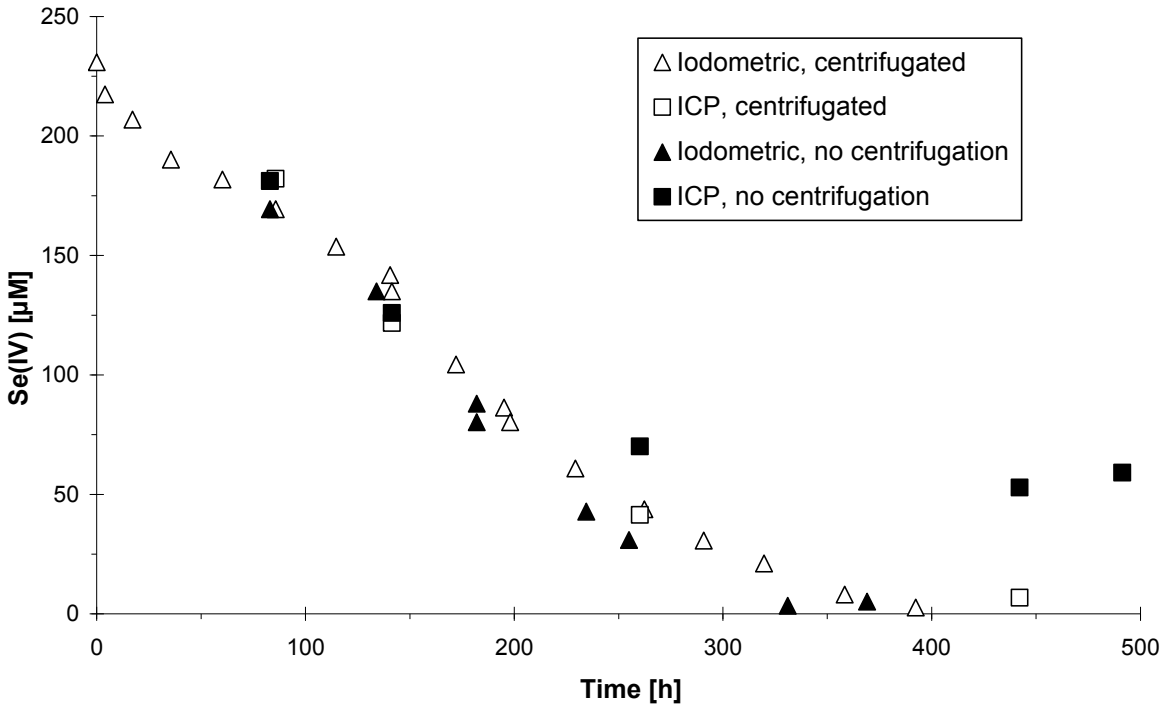

Figure 8: Comparison of iodometric and ICP results with and without prior centrifugation for 1.25 mg Pd/ml, 24 bar H_2

The centrifuged ICP and iodometric samples give very similar results, demonstrating that iodometry was able to successfully measure the concentration of dissolved selenium, and that selenite was the dominant dissolved selenium component. In the selenite conversion range 0-80%, the ICP analysis with and without prior centrifugation yielded the same results. At higher conversions, the uncentrifuged ICP results gave higher measured Se concentrations than the centrifuged samples. We attribute this to the formation of colloids undetectable by iodometry and large enough to be removed by the centrifugation. If significant quantities of free selenide were formed in solution, this would have suppressed the iodometric but not the ICP results, regardless of centrifugation. Since this was not observed, any amount of dissolved selenide in the solutions must have been low.

There is growing evidence that the UO_2 matrix of the SNF can act as a co-catalyst enhancing the effective catalytic surface around the metallic particles. As can be seen in Figure 9, the rate of selenite removal was dramatically increased either when dissolved uranyl was added simultaneously with the selenite or when the uranyl was added and allowed to reductively precipitate prior to the addition of selenite. H_2 is known to rapidly reduce dissolved uranyl into uranium dioxide in the presence of Pd(s) under conditions similar to those used in this work [76]. The rate of uranyl immobilization was orders of

magnitude higher than the selenite immobilization and is not shown in Figure 9. However, dissolved selenate, Se(VI), remained in solution under the present conditions, with no sign of adsorption or reduction by H_2 either in the presence of Pd (not shown) or in the presence of Pd with uranium dioxide with or without carbonate or sodium chloride in solution.

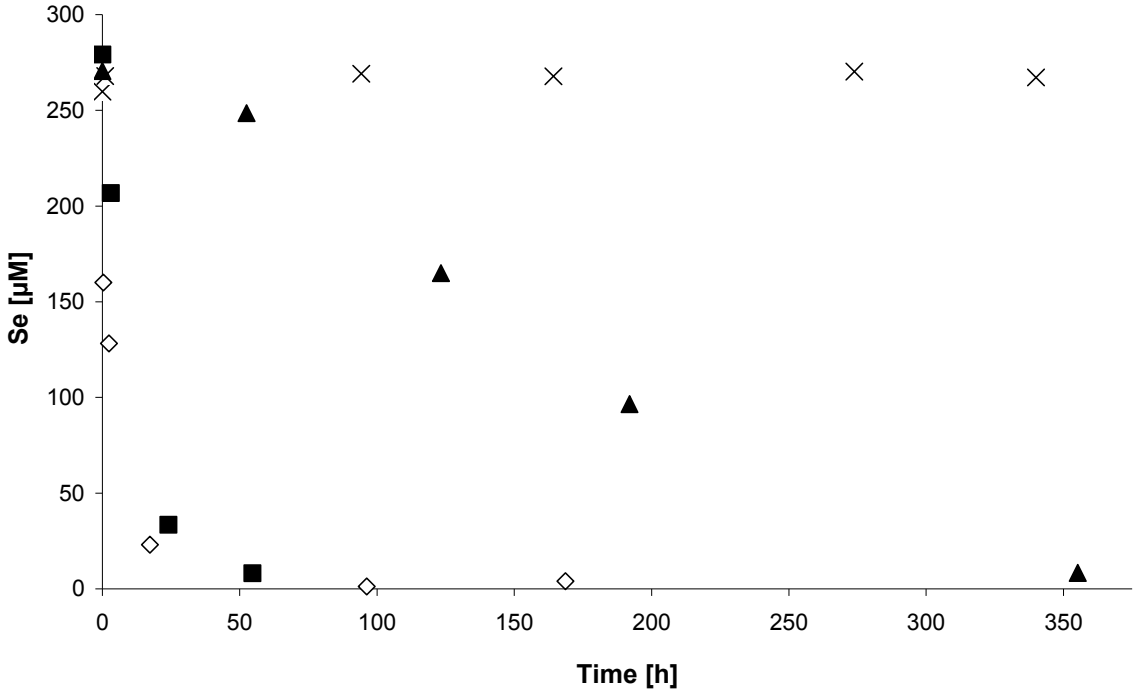

Figure 9: Comparison of kinetics, 0.45 mg Pd/ml, 24 bar H_2, 10 mM $NaHCO_3$, 10 mM NaCl. ×**:** 270 µM Se(VI) + 420 µM U(VI). ▲**:** 270 µM Se(IV). ■**:** 270 µM Se(IV) + 420 µM U(VI). ◊**:** 270 µM Se(IV) + pre reduced uranium equivalent to 420 µM U(VI).

The possible synergistic effect of Pd and UO_2 on the immobilization of selenite under hydrogen was also investigated by the use of UO_2 pellets, doped with 0.1%, 1% and 3%-wt Pd-particles in solution under H_2 atmosphere. The conditions of the Pd-UO_2 pellet experiment is presented in Table 2

Table 2: Details for the Pd-UO_2 pellet experiments. All samples contains 10 mM NaCl, 10 mM $NaHCO_3$ and 250 μM Na_2SeO_3. The labeling refers to the Pd-content of the UO_2 pellet and the H_2 pressure (in bar).

Sample	Pd-fraction [%-wt]	H_2 pressure [bar]
0.1-10	0.1	10
1-1	1	1
1-10	1	10
3-1	3	1
3-10	3	10

As can be seen in Fig. 10(a) for sample 3–10, the rate of selenite removal was considerably higher than for sample 1–10, followed by sample 0.1–10 which displayed the slowest reaction dynamics. Sample 0.1–10 reaches a plateau after removal of ~40% of the selenite, possibly due to blockage of the surface or poisoning of the Pd catalyst. Poisoning of Pd catalysts is documented for reduced sulfur species [77] which could be suspected to behave in an analogous way to reduced Se species.

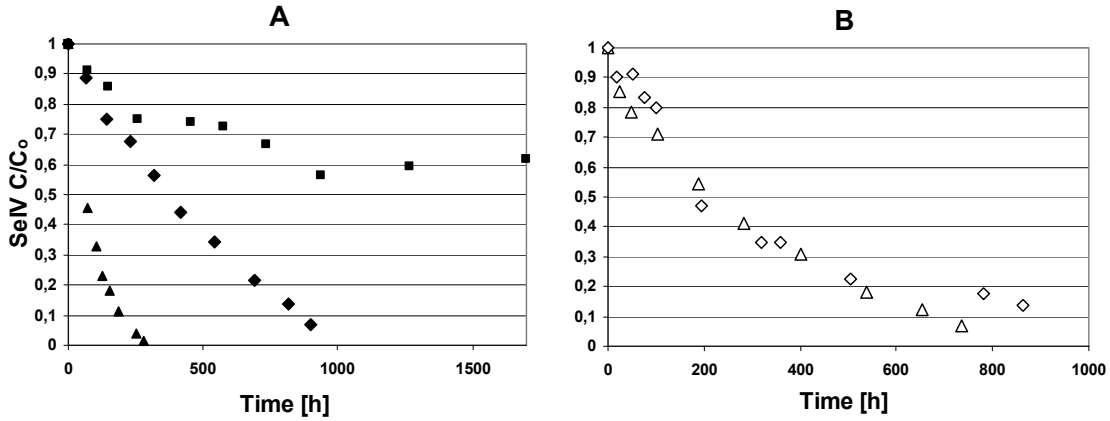

Figure 10a-b: Normalized Se(IV) concentrations vs. time. (a) 10 bar H_2: ▲, 3% Pd; ♦, 1% Pd; ■, 0.1% Pd. (b) 1 bar H_2: Δ, 3% Pd; ◊, 1% Pd. The analytical error is estimated to ~10%.

Data on Se poisoning of Pd catalysts is however scarce, although it has been observed for organic Pd catalysts [78]. The experiments performed (Figure 10b) at 1 bar H_2 resulted in approximately the same rate for the 1%-Pd pellet but with a considerably slower reduction of Se(IV) for the 3% Pd-pellet compared to the experiments at 10 bar H_2.

The selenite concentration remained constant for >2000 hours in a parallel experiment using a UO_2 powder suspension under 25 bar H_2 pressure (same solution composition as

in the pellet experiments) where the solid surface area to solution volume ratio was higher than in the pellet experiments (not shown). This indicates that Pd is the critical component for Se(IV) reduction to occur and that Se(IV) adsorption on UO_2 is very limited under the present conditions. When less than 5 % of the initial selenite concentration remained in sample 3-10 the previously transparent solution turned faint orange/red with a small amount of red particles on the bottom of the vessel, indicating that colloids had formed.

PCS, Photon Correlation Spectroscopy was used to verify the existence of colloids in the solutions from the 10 bar H_2 experiments after ~1500 hours reaction time. The sample solutions were transferred out of the glove box and measured immediately. Significant amounts of colloids were detected in samples 1-10 and 3-10. However, due to the lack of reference material the amount of colloidal material could not be quantified.

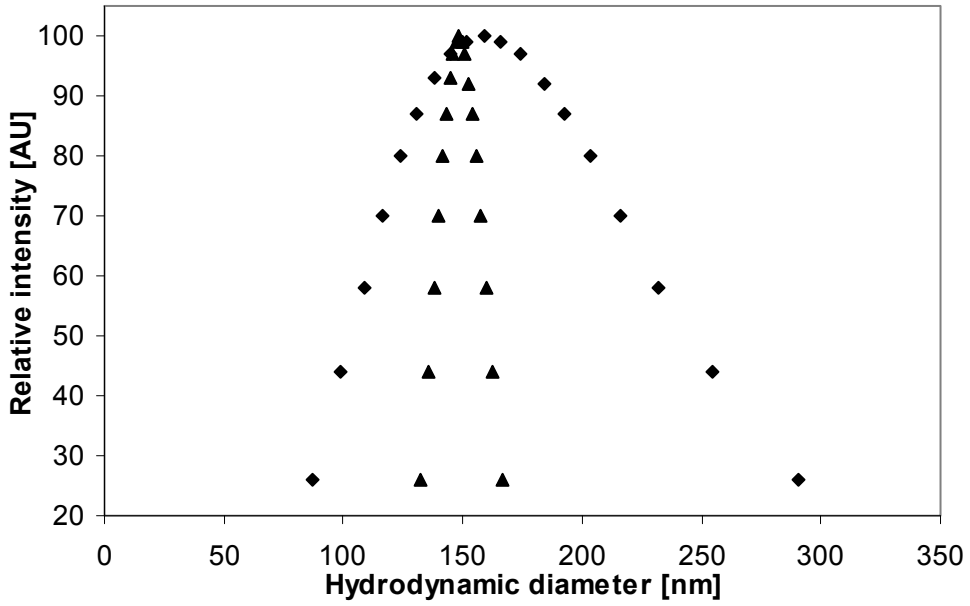

Figure 11: PCS size distribution of 10 bar H_2 samples at ~1500 h. ▲: 3%-Pd, 1.4 Mcps. ♦: 1%-Pd, 627 kcps. Background count rate: ~30 kcps.

As can be seen in Figure 11 the hydrodynamic diameter was around 150 nm for samples 1-10 and 3-10. The colloid concentration in sample 0.1-10 was too low as to allow a qualitative size distribution. It should be noted that the relative intensity scale in Figure 11 only relates to the size distribution of the individual sample and cannot be used to compare amounts of colloidal particles between samples. Centrifugation (RCF 25000 g) of the solutions removes all detectable colloids giving bright red precipitates. The

colloids were also studied by TEM. Solutions from the experiments were diluted by distilled water and a few drops were applied to and left to dry on copper TEM grids (in the dry anoxic atmosphere of the glove box). Particles of ~50-100 nm diameter were present in the TEM samples, as can bee seen in Figure 12 showing a picture from sample 0.1-10.

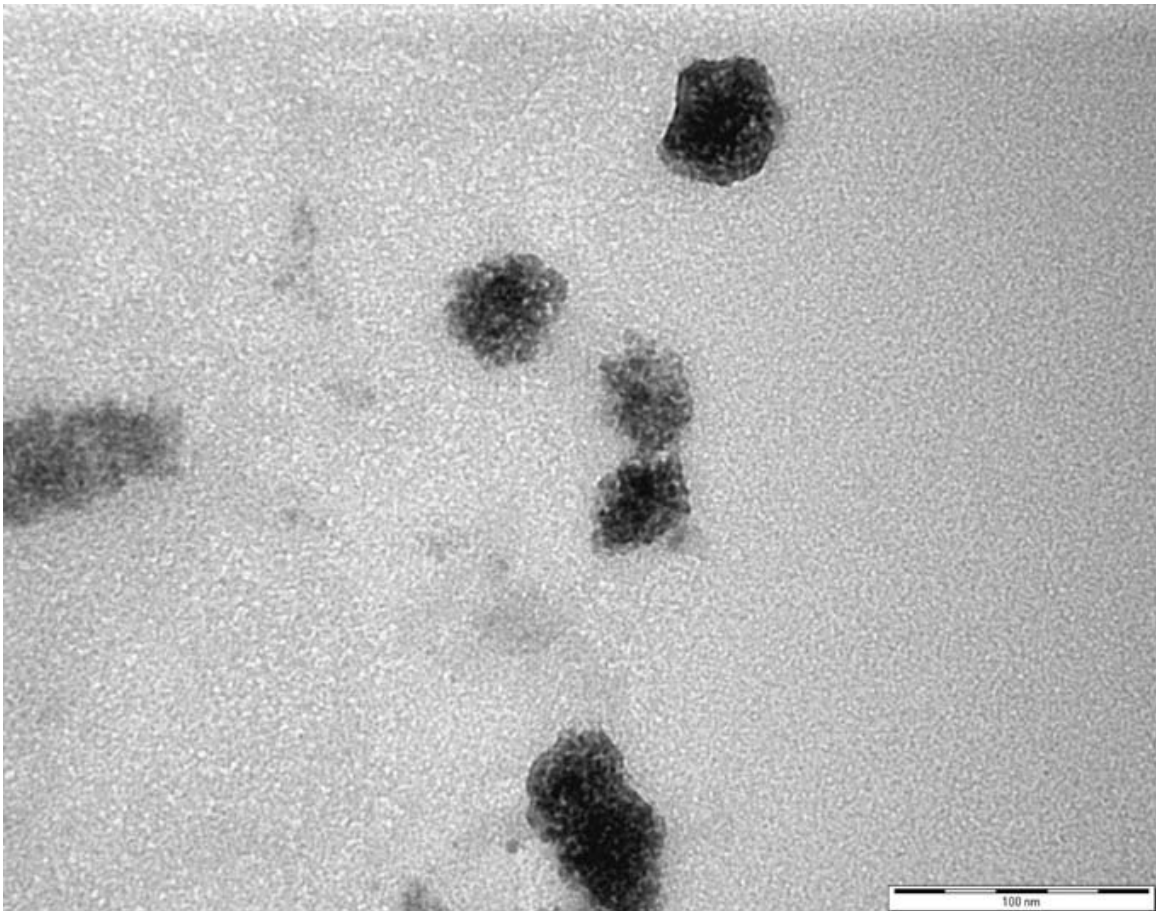

Figure 12: TEM image of colloids from sample 0.1-10.

Selected area electron diffraction of the particles did not yield any distinctive patterns, indicating that the particles are likely amorphous. Powder X-ray diffraction of the red precipitate from experiments (dried in the glove box) also lacked any distinctive reflexes, supporting the case that the product is amorphous.

Samples of the dried in colloidal solutions and precipitates were also investigated by Raman spectroscopy. The main feature of the spectra of the red solids is a strong band at ~255 cm^{-1} (Figure 13). Measurements on a predominantly monoclinic elemental selenium standard (confirmed by XRD measurement) displayed a band at ~253 cm^{-1}. A difference of 2 cm^{-1} is assumed to be within the limits of the spectral resolution of the instrument.

The differentiation between Raman bands from amorphous and monoclinic elemental Se allotropes is however difficult since amorphous Se is also assigned positions at ~250-255 cm^{-1} [74, 75].

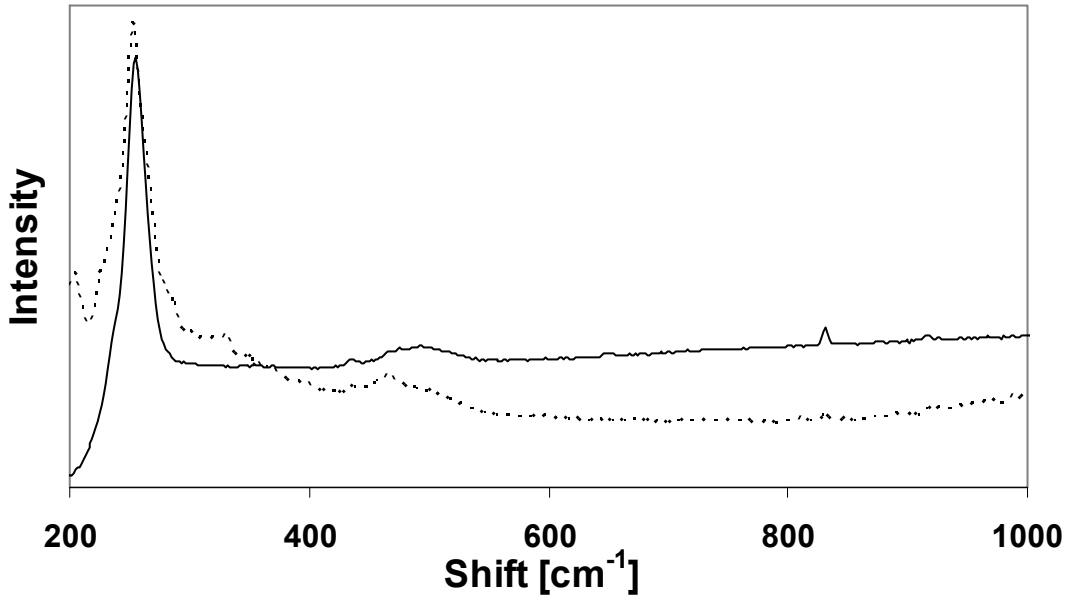

Figure 13: Raman spectra of red particles from sample 3-10 (solid line) and elemental Se-reference (dotted line).

Further evidence of elemental selenium in the investigated samples is the partial photoinduced transformation of the assigned elemental Se bands at ~253-255 cm^{-1} to trigonal elemental selenium (band at ~237 cm^{-1}) [74] that occurs in the samples as well as for the Se reference material after prolonged laser illumination (Figure 14). The pellet from sample 3-10 was removed from its solution and allowed to dry inside the glove box and fixated on a SEM-template with copper tape. SEM-EDS mapping of the pellet surfaces (Figure 15) revealed Pd-grains in the uranium dioxide matrix. No selenium was detected on the surface of the pellet indicating either very limited attachment of selenium to the surfaces, or that a selenium layer is of such thickness that it is undetectable by SEM-EDS.

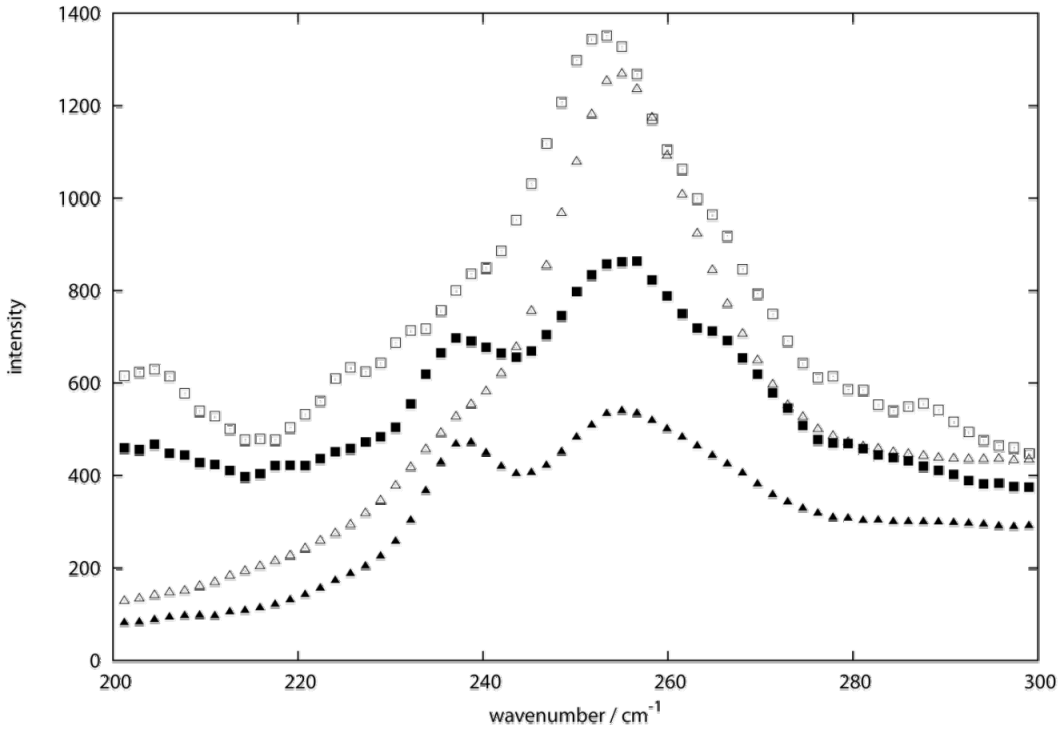

Figure 14: Raman spectra of the effect of prolonged illumination on sample 3-10 and the Se reference. □: Se reference. Δ: Sample 3-10 ■: Se reference after prolonged illumination ▲: Sample 3-10 after prolonged illumination.

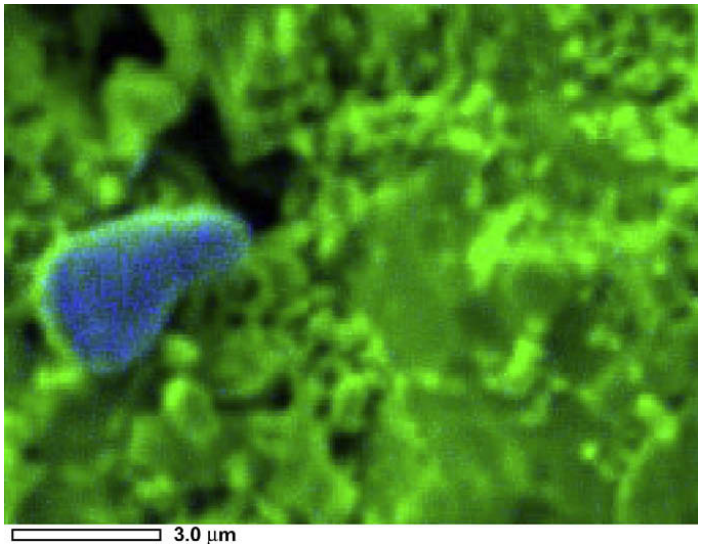

Figure 15: Bicolour SEM-EDS map of sample 3-10. Uranium (Green). Palladium (Blue).

Using the rates of reduction in the experiments and assuming the surface area of the pellets to be three times the geometric surface area, the overall rate constant for the pellet (in m s^{-1}) was determined. By plotting the overall rate constant against the Pd fraction, the second order rate constant for the Pd-catalyzed reduction was determined. There is a linear correlation between the rate constant (expressed as a second order rate constant on

the basis of the total surface area) and the Pd fraction (Figure 16), corresponding to a second order rate constant of 2.5±0.3 x 10^{-7} m s^{-1} with respect to the Pd surface area for the experiments at 10 bar.

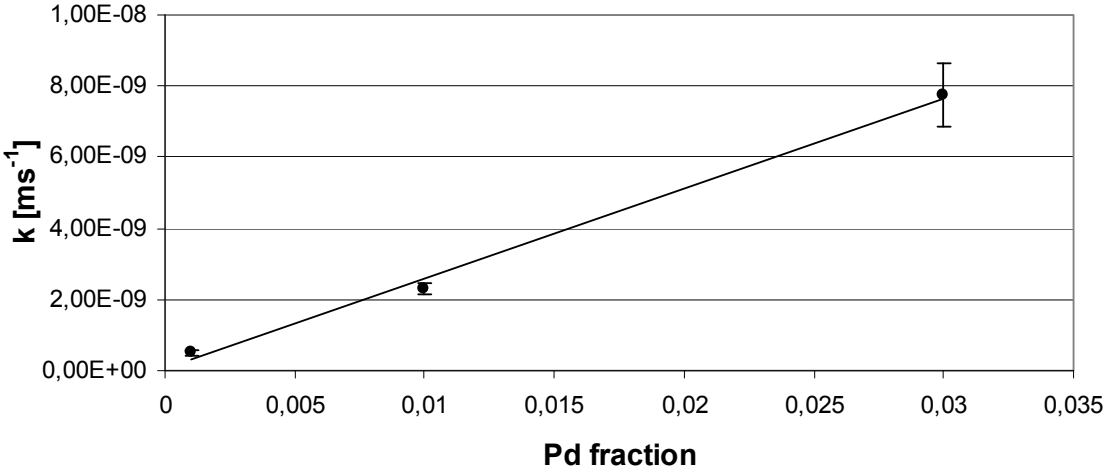

Figure 16: Second order rate constants for the selenite reduction vs. Pd fraction in the Pd-UO_2 pellets under 10 bar H_2

Due to the heterogeneous and autocatalytic nature of the Pd-powder suspension system, it is not a straight forward process to determine the reaction order and rate constant for the selenite reduction in this system. The maximum rate constant with respect to Pd content can nevertheless be estimated from the maximum slope in the Pd-powder experiments without uranium (Figures 5, 6). The reaction is assumed to be first order with respect to selenite and Pd. The resulting second order rate constant with respect to the Pd surface area is 1.2 ± 0.8 x 10^{-9} m s^{-1} if the surface area is calculated in the same fashion as for the Pd-UO_2 pellets (i.e. three times the geometrical surface area, assuming spherical 1.25 μm particles in this case). Given the BET surface area of the Pd-powder (1.12 m^2/g), which is ~2.80 times the geometrical surface area, this assumption seems appropriate. The rate constant for the Pd-powder suspensions under 24 bar H_2 (1.2 ± 0.8 x 10^{-9} m s^{-1}) was thus found to be about two orders of magnitude lower than for the UO_2 pellets (2.5±0.3 x 10^{-7} m s^{-1}) under 10 bar H_2, with respect to the Pd surface. The rate constants for the Pd-powders suspensions in the presence of reductively precipitated uranyl fall in between these rates (~6 ± 3 x 10^{-8} m s-1). Table 3 summarizes the calculated rate constants. Hence, it appears that the UO_2 matrix had a significant impact on the selenite removal kinetics.

Table 3: Second order rate constants for selenite removal

Rate constant [m s^{-1}]	**Conditions**
(1.2 ± 0.8) x 10^{-9}	Average of 0.15, 0.85, 1.25, 3.2 mg Pd/ml, 24 bar H_2, Figure 5
~2 x 10^{-9}	2nd Se(IV) injection 0.85 mg/ml Pd, 24 bar H_2, Figure 6
(2.5 ± 0.3) x 10^{-7}	3% Pd-UO_2 pellet, 10 bar H_2, Figure 16
(6 ± 3) x 10^{-8}	0.45 mg Pd/ml, Uranyl, 24 bar H_2, Figure 9
(6 ± 3) x 10^{-8}	0.45 mg Pd/ml, UO_2, 24 bar H_2, Figure 9

Comparison of the Pd-UO_2 pellets rate constant for selenite reduction at 10 bar H_2 with the previously determined one [79] for hydrogen peroxide (at equivalent hydrogen pressure, and with the same pellets) gives a difference of nearly two orders of magnitude lower for the selenite case. The reduction of selenite is, thus, significantly slower and far from being diffusion controlled under these conditions. (The hydrogen peroxide rate constant was found to be at the level of diffusion control).

From a thermodynamic perspective, both selenite and selenate should be reduced to elemental Se or selenide by H_2 (Table 4). No reduction of selenate was however observed in the experiments.

Table 4: Standard reduction potentials and calculated equivalent reduction potentials at pH 8.5, using the Nernst equation.

Standard process	**E_0 [V]**	**Calculated E_0 at pH 8.5 [V]**	**Reference**
$SeO_4^{2-} + 2H^+ + e^- \rightarrow SeO_3^- + H_2O$	-0.03	-1.03	[81]
$SeO_3^- + H^+ + e^- \rightarrow HSeO_3^-$	2.18	1.68	[81]
$HSeO_3^- + 5H^+ + 4e^- \rightarrow Se + 3H_2O$	0.78	0.15	[64]
$Se + H^+ + 2e^- \rightarrow HSe^-$	-0.23	-0.48	[64]
$Se + H^+ + 2e^- \rightarrow HSe^-$	~ -0.1	-0.35	[83]
$2H^+ + 2e^- \rightarrow H_2$	0	-0.5	-

A number of studies have demonstrated that selenate is notably harder to reduce than selenite [58, 63, 80]. One explanation for this difference can be found in the work of Kläning and Sehested [81], in which they determined the potential barrier imposed by intermediary Se(V) in the stepwise one-electron reduction of Se(VI) to Se(IV), as can be seen in Table 4. From the thermodynamic data in Table 4, it can be concluded that it either takes a very strong one-electron reductant or a two-electron reduction process to reduce selenate to selenite at pH ~8.5. To test this conclusion, a simple radiation chemical experiment using an electron accelerator was performed. By adding N_2O and 2-PrOH, the solvated electron and the hydroxyl radical (a radiolysis product of water) can be quantitatively converted into $HO(CH_3)_2C^{\bullet}$, which is a considerably weaker reductant than the solvated electron itself [82]. Two types of experiments were performed, with duplicate samples. In the first type, selenite and selenate were reduced by $HO(CH_3)_2C^{\bullet}$, while in the second type the solvated electron was used as the reductant by bubbling the solutions with Ar instead of N_2O and by replacing 2-PrOH with t-BuOH. Tertiary butanol scavenges hydroxyl radicals without producing a reducing radical. The results are presented in Table 5.

Table 5: Percentage of Se remaining in the aqueous phase after irradiation, extraction and centrifugation. A and B refer to duplicate experiments.

Se-speciation	**Reductant**	**A [%]**	**B [%]**
Selenate, Se(VI)	e^-_{aq}	7.2	10.3
Selenate, Se(VI)	$HO(CH_3)_2C^{\bullet}$	97.2	92.7
Selenite, Se(IV)	e^-_{aq}	3.6	0.5
Selenite, Se(IV)	$HO(CH_3)_2C^{\bullet}$	6.9	0.8

As can be seen from Table 5, selenite was efficiently reduced in both systems, while only the solvated electron was capable of reducing selenate. This is in agreement with the thermodynamics of one-electron transfer. Since no reduction of selenate occurs in the H_2/Pd system, the adsorbed hydrogen on the catalyst appears to be dissociated to hydrogen atoms operating as stepwise one-electron reductants. The standard potential of the hydrogen atom is insufficient to overcome the thermodynamic one-electron barrier to reduce selenate under the present conditions. Bearing in mind that this is a heterogeneous system, it should be noted that the apparent lack of selenate adsorption on the catalyst may also be a limitation.

Selenite was found to be reduced to elemental Se, with only some indirect evidence of selenide (HSe^-) formation. The latter is the expected thermodynamic end product, although it should be stressed that there is some uncertainty in the reduction potential of elemental Se (Table 4, references 64, 83). It is also possible that selenide formation is kinetically limited, and perhaps suppressed by its reaction with selenite, yielding elemental Se as long as any selenite is present [73]. The formation of polyselenide species such as Se_x^{2-} and/or the radical species Se_x^- in the transition between Se(0) and Se(-II) is also a possibility [84]. It should be stressed that dissolved selenides are very sensitive to oxidation by air [85]. Furthermore, the selenide anion adsorbs readily to colloidal elemental selenium [86], possibly masking any selenide formation. Various attempts were made to identify selenide in samples taken directly from the autoclave (under anoxic conditions). Separation by strong acidification, evolution of H_2Se followed by scrubbing and precipitation of evolved H_2Se, or direct moderately acidic precipitation of sparingly soluble selenides such as copper selenide yielded only minute amounts of precipitate (unidentifiable by either Raman or XRD) other than elemental Se. Hence, no direct evidence of selenide formation was obtained.

Further studies are required in order to fully identify the mechanism behind the observed auto-catalytic process responsible for the reduction of selenite. In the context of spent nuclear fuel repositories, the Pd-containing noble metal inclusions are likely to be effective catalysts for the H_2 reduction of potentially mobile radioactive selenite into sparingly soluble elemental selenium. This study also offers evidence that the combination of Pd and UO_2 enhances the catalytic effect of Pd under hydrogen conditions which is also of interest in the nuclear fuel repository context.

It is interesting to note that Pd(s) does not appear to be an effective catalyst for selenate reduction by hydrogen. The demonstrated difference between selenite, Se(IV), and selenate, Se(VI), in sensitivity towards stepwise one-electron reduction, which we attribute to the one-electron reduction potential barrier imposed by intermediary Se(V), may also offer an explanation for the difference between Se(IV) and Se(VI) observed in previous studies concerning reductive immobilization of selenium oxyanions.

Selenium immobilization by iron and corrosion products under anoxic conditions and the influence of uranyl (Paper III, IV)

Many SNF repository designs such as the Swedish KBS-3 [87] rely on burial of the SNF in canisters deep under ground (~500 m below the surface) where the conditions are expected to be anoxic. In most of the SNF repository designs a large part of the SNF-canister is composed of iron, sometimes with additional engineered barriers such as an outer copper canister and bentonite clay (as in the KBS-3 concept). In order for the SNF to be exposed to the groundwater the canister must fail. The iron will thereby come in contact with anoxic groundwater and corrode before the SNF matrix can release fission products, such as ^{79}Se. Escaping radionuclides would thus come in close contact with the iron insert. Iron and certain iron corrosion products have been shown to reduce and thus immobilize dissolved selenite and selenate [88-94]. Data on the immobilization of selenate by iron and the effect of uranyl present in solution are however scarce. Since SNF is composed of ~95% UO_2, a large amount of uranium would have to dissolve in order for the SNF matrix to release significant amounts of fission products such as ^{79}Se. Given that any dissolved uranyl would likely be present as anionic dicarbonate, $UO_2(CO_3)_2^{2-}$ or tricarbonate, $UO_2(CO_3)_3^{4-}$ complexes or a mix thereof in carbonate rich groundwater one could expect it to compete with selenium oxyanions for both adsorption sites and reductive capacity of the corroding iron surfaces, potentially hindering the selenium immobilization. The effect of the presence of uranyl on the immobilization of selenium oxyanions is consequently of interest, especially given that uranyl hydroxide or carbonate complexes can be adsorbed by Fe(III) hydroxides [95] and also reductively immobilized by iron [96, 97], magnetite [98], and other iron corrosion products, such as green rusts, GR [99].

Magnetite, Fe_3O_4 is believed to be a likely major corrosion product formed on iron corroding under anoxic groundwater conditions [100, 101]. Studies have shown that selenite sorption on magnetite decreases with increasing pH. Selenate following the same trend, is less readily adsorbed [102], which is unfavorable at the expected pH of ~8 in carbonate rich groundwater. The situation is somewhat unclear as to whether selenite is reduced by magnetite. Recent work by Scheinost et al [93, 94] employing synthetic nanoparticulate magnetite under anoxic conditions demonstrated reduction of selenite to ironselenide phases at a pH of ~5. However, equally recent work also employing

synthetic nanoparticulate magnetite under anoxic conditions indicated no reduction of adsorbed selenite in the pH range of 4.8-7.9, [103]. The studied system is not only of interest in a deep SNF repository context but also share similarities with other nuclear waste forms such as tank or pond wastes from past reprocessing activities. Another related issue is pollution from uranium mining tailings, which among the major contaminants such as uranium also contains naturally occurring Se in levels of concern [104, 105]. These wastes are often disposed in or expected to migrate into areas where the conditions are anoxic, with iron being a common major element in containers or engineered reactive permeable barriers [106] installed in order to remediate contaminant release. In the experiments we examine the impact of dissolved uranyl on the immobilization of selenite and selenate by metallic iron or corroded iron surfaces with magnetite layers under simulated anoxic groundwater conditions. The focus is on examining the possibility for reductive selenium immobilization, as a consequence small surface to volume ratios are employed with rather high selenium and uranium concentrations in order to facilitate the surface characterization performed using Raman spectroscopy, SEM-EDS (Scanning Electron Microscopy Energy Dispersive X-ray Spectroscopy) μ-XRF (X-ray fluorescence) and μ-XAS (X-ray Absorption Spectroscopy). The solid surfaces used in this study are presented in Table 6.

Table 6: Solid surfaces employed in the study.

Designation	**Description**
N	Polished iron foils representing a pristine iron surface
UP	Iron foils precorroded in an anoxic uranyl solution at room temperature for 300 d prior to the experiments
HTP	Iron foils precorroded in anoxic water at 80˚C for 60 days prior to the experiments.
Iron powder	Iron powder (140 μm diameter), precorroded in anoxic water at 80˚C for 60 days prior to the experiments.
UO_2	UO_2 powder

The polished iron foils (N-samples) represents a pristine iron surface, the foils (UP) precorroded at room temperature in a uranyl solution simulate the case of iron that has been in contact with reducible contaminants (uranyl in this case) under otherwise anoxic conditions during an extended time (300 d). The foils and powder (HTP, iron powder) precorroded in hot anoxic water simulate the case of iron that has corroded to build up a comparatively thick magnetite corrosion layer. Finally the UO_2 powder sample was included to examine if a UO_2 surface would have any significant capacity to immobilize selenate.

Subsamples of the materials presented in Table 6 were characterized by Raman spectroscopy (Figure 17) prior to the experiments. The major band at 670 cm^{-1} in the Raman spectra for the iron foil precorroded in uranyl, and from the high temperature pre-corrosion agrees with the reported data for magnetite [107], indicating magnetite as the dominating species on the surfaces. It must be noted that the probing depth of the Raman analysis is estimated to be in the range of 0.5–1 μm [101]. A thin corrosion film of a different composition on the surface of the material could thus remain undetected if the bulk of the underlaying corrosion layer is composed of magnetite. The bands at 445 cm^{-1} and 1151 cm^{-1} on the bulk UO_2 material are consistent with close to stoichiometric UO_2 [108]. No uranium species was however detected by Raman analysis on the iron foil precorroded in uranyl despite the removal of all uranyl from solution and the appearance of black corrosion products covering the surface. We can only speculate that otherwise clear Raman bands of cubic UO_2 disappear with structural disorder and that the uranium species on the precorroded foil could likely be amorphous or nanoparticulate UO_2 with little to no Raman signal. Dark coloured corrosion products also absorb more of the laser light making Raman analysis difficult. No adsorbed uranyl (Raman band of UO_2^{2+} at ~870 cm^{-1}) could be detected on the surface of the foils precorroded in the uranyl solution. The polished iron foil without pre-corrosion lacked any distinctive Raman features.

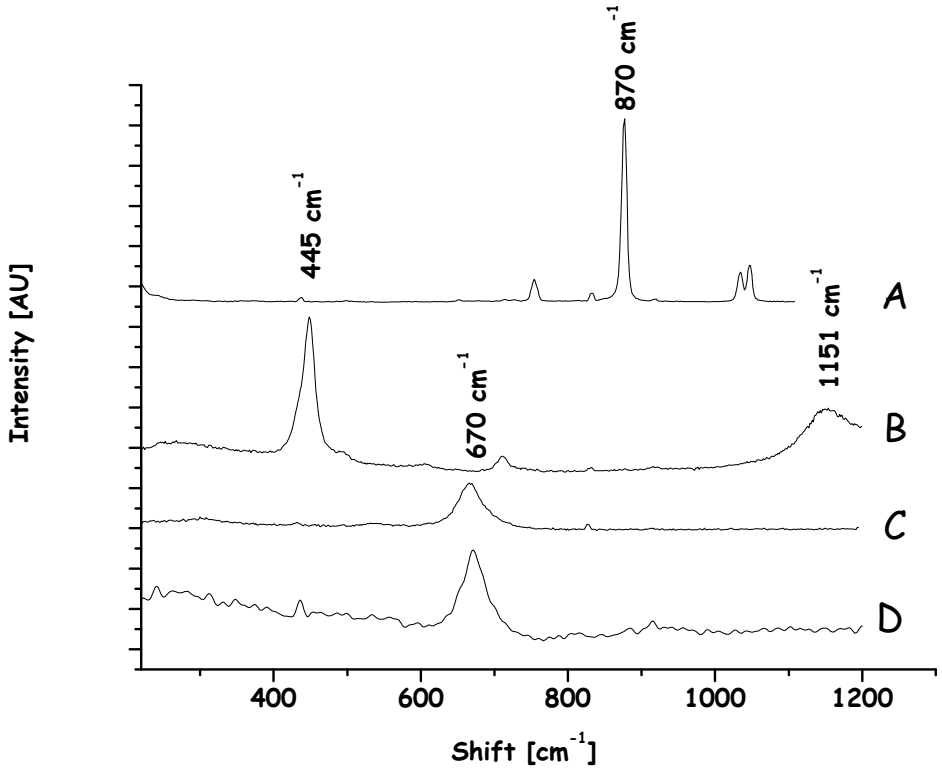

Figure 17: Representative Raman spectra of the precorroded materials: (A) uranyl nitrate, (B) UO_2 powder, (C) magnetite powder and (D) iron foil precorroded in uranyl solution.

The BET-surface area of a larger parallel batch of pre-corroded foils was measured (Micromeritics Flowsorb II 2300, He/N_2: 70/30). The detection limit of the instrument is ~0.1 m^2. Due to this limitation approximately 10 times more material than used in the actual experimental samples was used for the BET-surface area measurement of the polished foils with no pre-corrosion. Despite this the uncorroded iron foils (N-samples) did not show any detectable BET-area (<0.01 m^2). The bulk UO_2 powder has the BET-surface area of 5.85 m^2 (corresponding to 5.85 m^2/g). The uranyl precorroded foils, UP yielded a BET-surface area of ~0.72 m^2 and the high temperature precorroded foil, HTP had a surface area of ~0.1 m^2. Batch experiments were performed either in plastic bottles (50 ml solution) or in clear glass tubes to facilitate observation of the evolution of the corrosion products. The standard solution was composed of 10 mM NaCl, 2 mM $NaHCO_3$, pH ~8. All solutions were prepared inside the glove box (<0.1 ppm O_2, Ar + 0.03% CO_2) from degassed Milli-Q deionized water (18 MΩ). The selenate used (Na_2SeO_4, Alfa Aesar, 99.8%) was analyzed iodometrically to test for any selenite

contamination of which none could be detected. The selenium and uranium concentrations in solutions were measured by ICP-OES. The selenite was also analyzed both iodometrically and by ICP and was found to be selenate free. The conditions for the batch experiments are presented in Table 7. For the surface characterization small subsamples were removed from each sample solution, briefly dipped in deionized water followed by ethanol in the glove box. Analysis of the rinsing solutions did not indicate any removal of Se or U by these steps. After drying the subsamples were either cast in epoxy and polished or fixated on kapton tape for SEM-EDS and XAS analysis. The samples for Raman analysis were sealed under a thin cover glass.

Table 7: Summary of samples, pretreatment, selenium and uranyl concentrations. The first letter in the sample name indicates the type or pretreatment followed by the initial concentration in μM and selenium speciation, and lastly the initial uranyl concentration in μM (N: No pre-corrosion, UP: 300 d at 25°C in initial 0.42 mM U(VI), HTP: 60 d at 80 °C, UO_2: UO_2 powder, no iron).

Sample	**Se [μM]**	**U-VI [μM]**
N250SeVI	250 SeVI	-
N250SeVI/420U	250 SeVI	420U
UP250SeVI	250 SeVI	-
UP250SeVI/420U	250 SeVI	420U
$UO_2$250SeVI	250 SeVI	-
HTP250SeIV	250 SeIV	-
HTP250SeVI	250 SeVI	-
HTP250SeIV/420U	250 SeIV	420
HTP250SeVI/420U	250 SeVI	420

The concentrations of Se and U in the experimental solutions were measured as function of reaction time (the analytical error is estimated to 1-10 μM). The pH was measured at the start and end of the experiments and remained constant at pH ~7 for the samples containing uranyl and pH ~8 for the sample with no addition of uranyl. A reference solution containing 10 mM NaCl, 2 mM $NaHCO_3$, 0.25 mM selenate and 0.42 mM uranyl was included. The stable levels of Se and U of this solution indicate no or very limited sorption to the vessel or precipitation under the present conditions (Figure 18a).

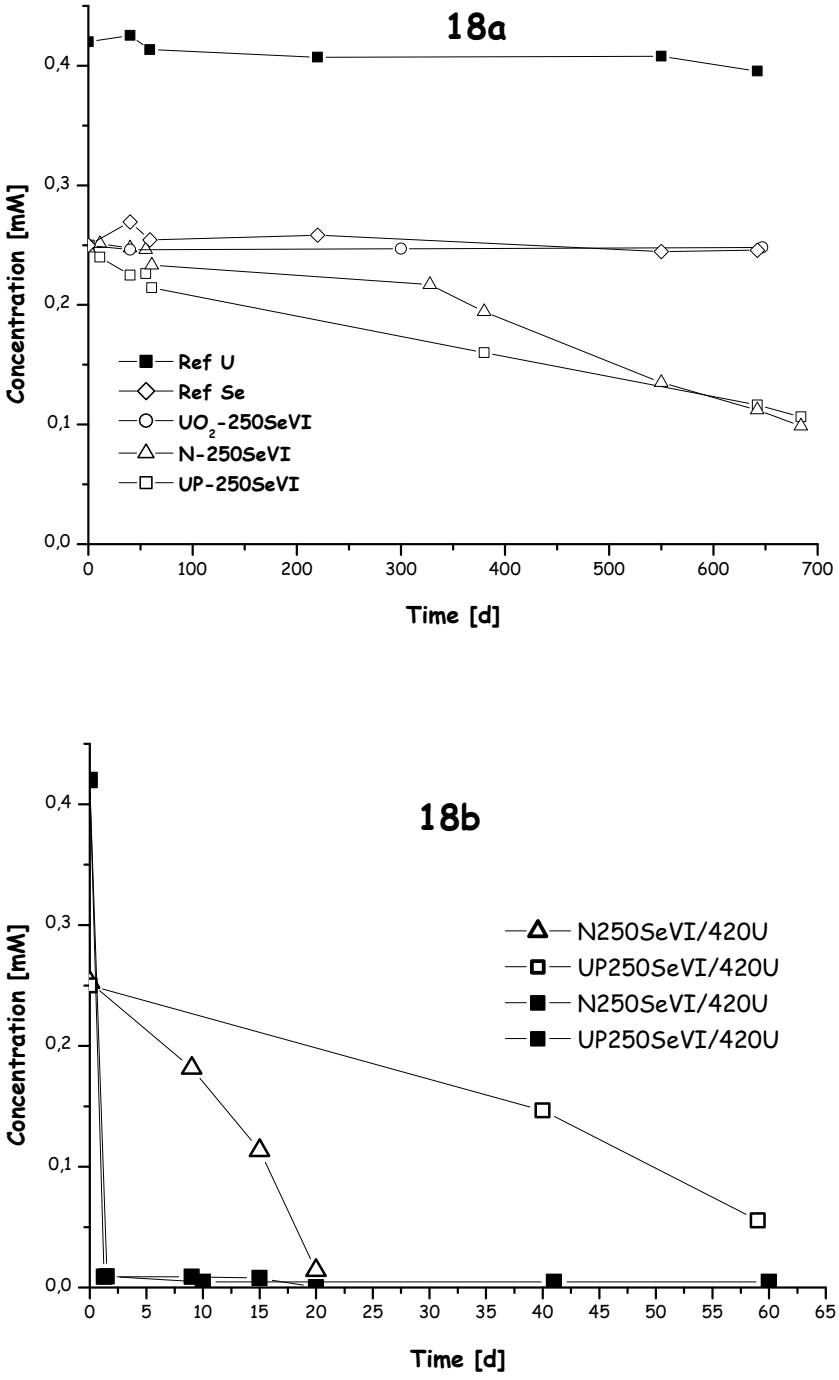

Fig. 18. (a–b) Immobilization dynamics of the N and UP and UO_2-sample. Open symbols represent Se concentrations, closed symbols are U-concentrations.

From the samples where a solid substrate is present we can see that the Se concentration decreases very slowly for the polished iron foil (sample N-250SeVI, Figure 18a). When uranyl and selenate are added simultaneously, the Se concentration decreases rapidly in

the presence of a polished iron foil (sample N-250SeVI/420U). When a polished iron foil is pretreated with uranyl (300 days prior to the addition of selenate) only a slight increase in the initial rate of Se concentration reduction is observed (sample UP-250SeVI/420U, Figure 18a) compared to the experiment where no uranyl was added. When more uranyl was added to the solution the rate of Se concentration reduction increased considerably (sample UP-250SeVI/420U, Figure 18b) reaching similar values as in sample N-250SeVI/420U, Figure 18b. No significant reduction in Se concentration was observed over 684 days in the pure UO_2 powder sample, UO_2-250SeVI (Figure 18a). This indicates that the nature of the uranyl effect is transient and that UO_2 itself is most likely not the active reagent. Comparing the rates of Se immobilization of UP-250SeVI and N-250SeVI/420U which both have similar surface areas and UO_2-250SeVI which has a significantly larger BET-surface area the increase in surface area itself does not appear to govern the rate of Se-immobilization.

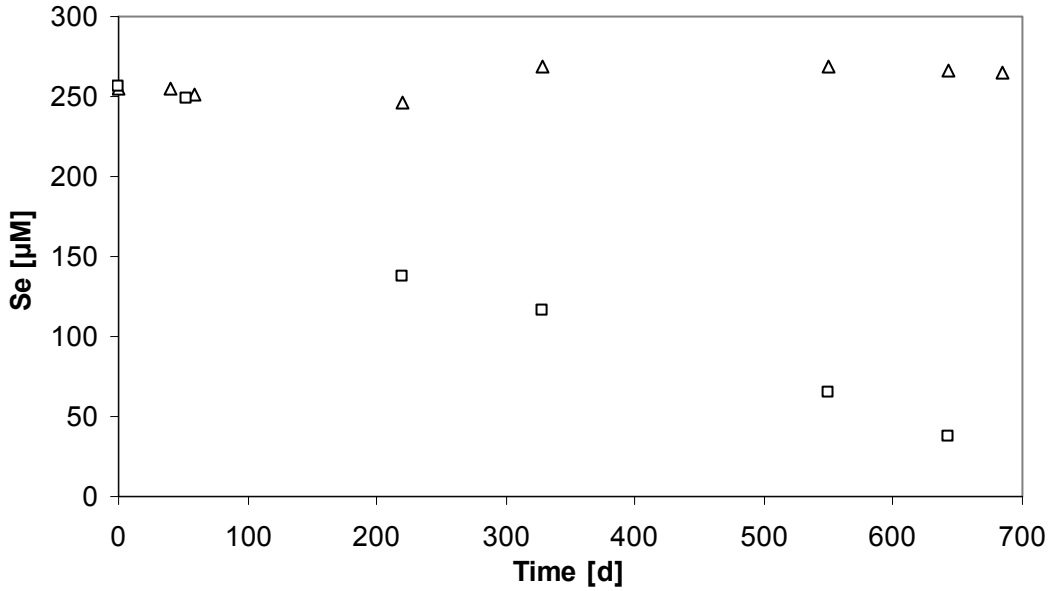

Figure 19: Evolution of the Se concentration in samples HTP-SeIV250 (□) and HTP-SeVI250 (Δ).

For sample HTP-250SeVI no significant change in Se concentration was observed whereas the Se is slowly immobilized in sample HTP-250SeIV (Figure 19).

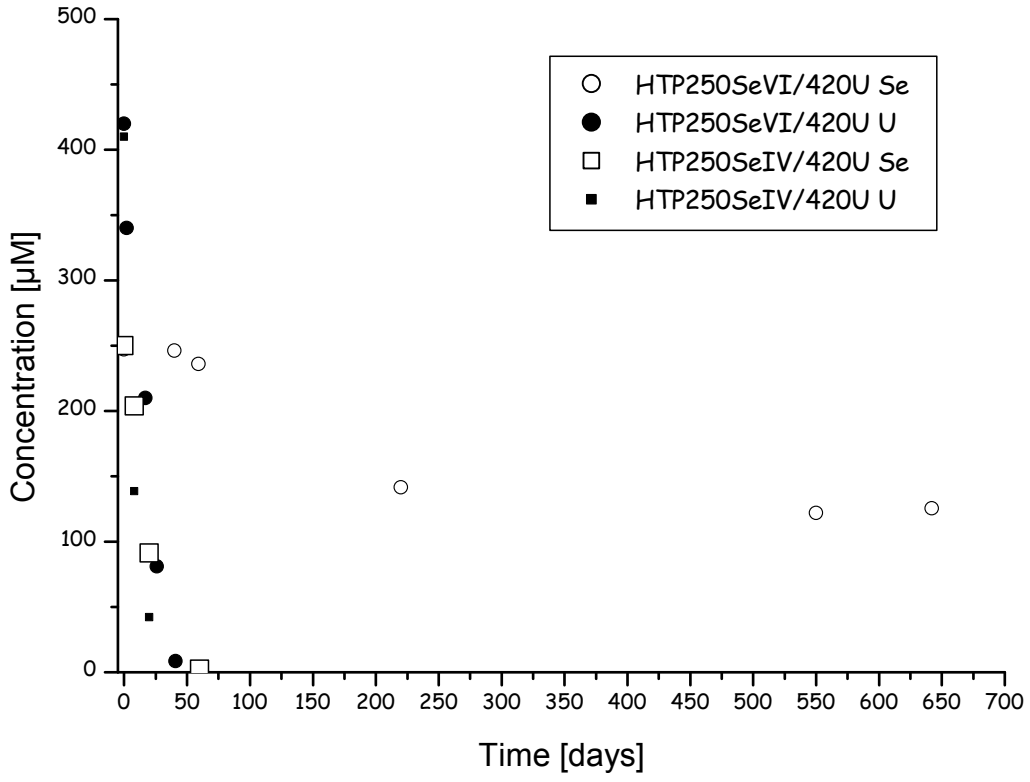

Figure 20: Evolution of Se and U concentrations in samples HTP-250SeIV/420U and HTP-250SeVI/420U. Open symbols for Se concentrations and filled for U.

For the samples HTP-250SeIV/420U and HTP-250SeVI/420U the uranium is immobilized within 40 days (Figure 20). The removal of uranyl was associated with formation of a voluminous corrosion product that was only weakly attached to the foils. The appearance of, or level of corrosion products on the samples without any uranyl (samples HTP-250SeIV and HTP-250SeVI) did not appear to change over the course of the experiment. The selenite in sample HTP-250SeIV/420U was completely immobilized within the same time frame as the uranyl (Figure 20). The selenate in sample 250SeVI/420U decreased at a much lower rate reaching an apparent plateau level at ~125 µM, approximately half of the initial concentration (Figure 20). The removal of selenate, and most notably, that of the uranyl is considerably slower for the HTP samples compared to the N and UP samples. The lower immobilization rate indicates that the presence of the magnetite corrosion layer decreased the reactivity of the iron surface.

The samples from the batch experiments were found to have a rather heterogeneous speciation. Raman spectroscopy indicates the presence of the iron corrosion product magnetite (strong band at 670 cm^{-1}) on all iron containing samples and to a lesser degree maghemite and hematite. Evidence for a very heterogeneous spatial distribution of elemental Se was obtained for sample N-250SeVI/420U (Figure. 21) where the intensity of the band at 236 cm^{-1} (corresponding to the stretching mode of trigonal zero-valent Se [74], varied significantly between different spots.

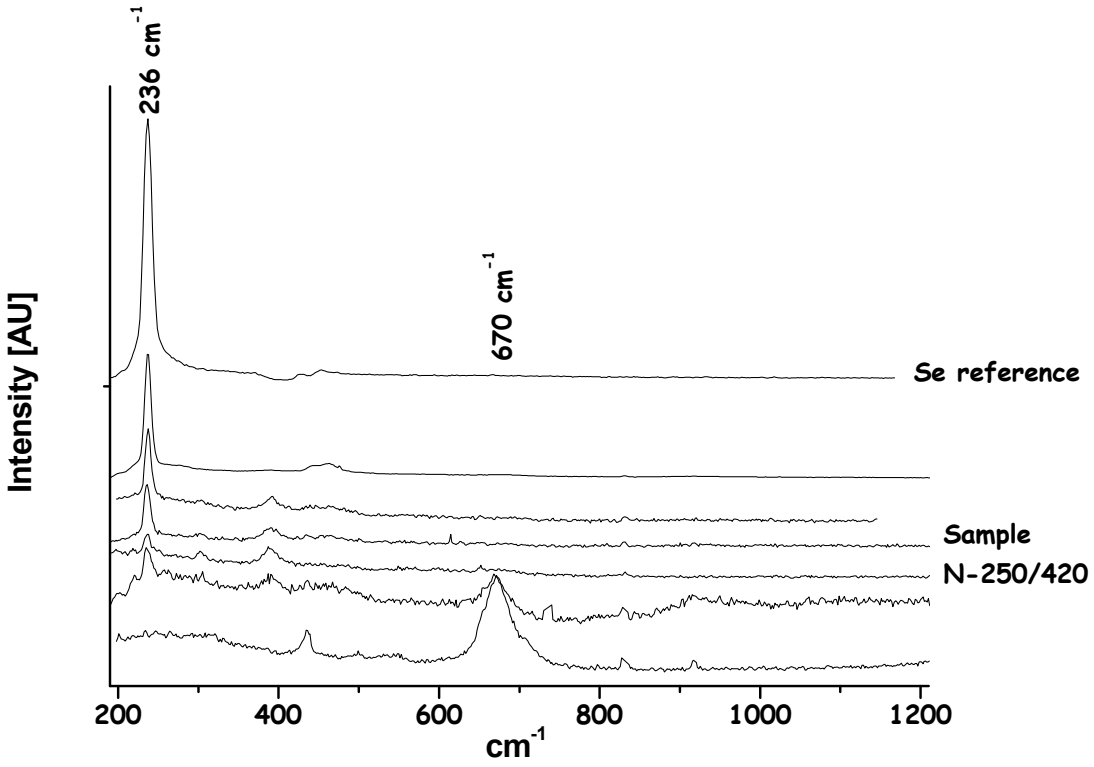

Figure 21. Raman spectra of 6 regions on sample N-250SeVI/420U and the elemental Se reference (upper spectra).

Raman bands at 236 cm^{-1}, evidence of elemental Se was also observed on sample UP-250SeVI/420U (Figure. 22), as well as several iron oxides, the band at 670 cm^{-1} in the middle spectra is assigned to magnetite (Figure. 22), the broadened band at ~716 cm^{-1} is assigned to maghemite and the bands at 1308 and 296 cm^{-1} are assigned to hematite (Figure. 22).

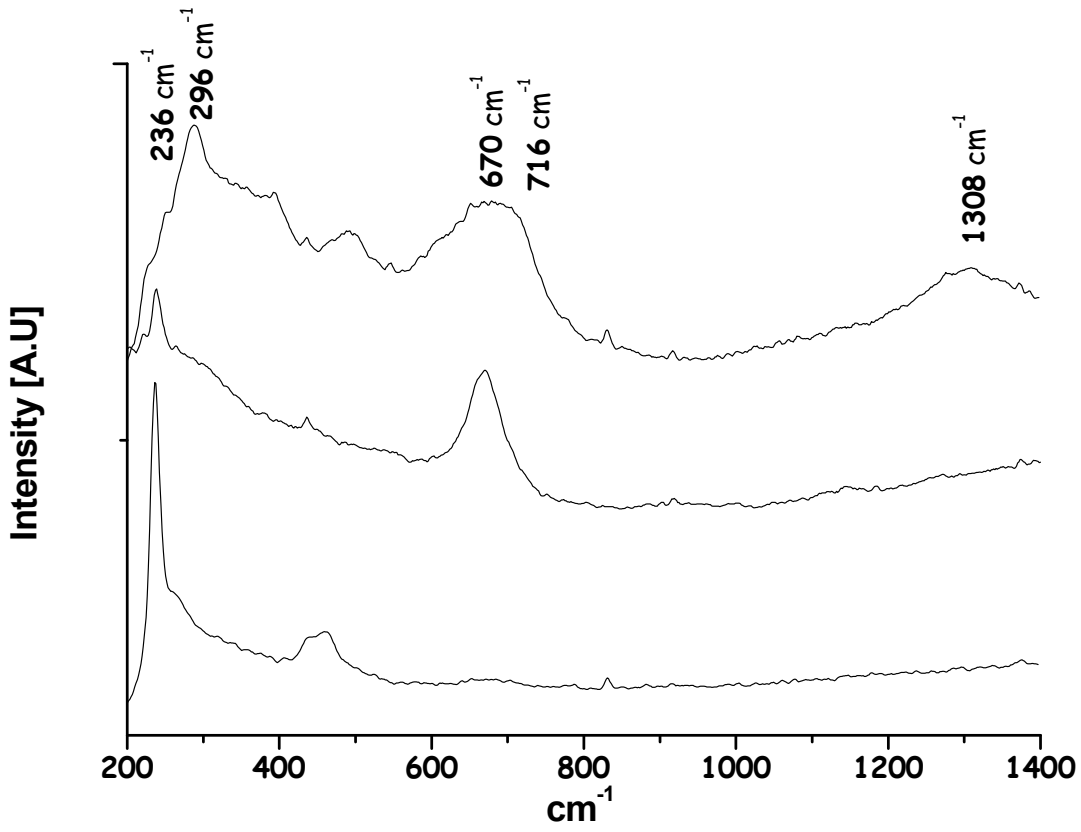

Figure 22: Raman spectra from three regions on sample UP-250SeVI/420U.

Raman spectra from sample N-250Se (Figure. 23) also indicate significant presence of magnetite, maghemite and hematite. The strong band at 256 cm^{-1} in the middle spectra and partly in the lower spectra in Figure. 23 could be attributed to monoclinic or amorphous elemental selenium, or a mixed allotropy of elemental selenium [109, 110].

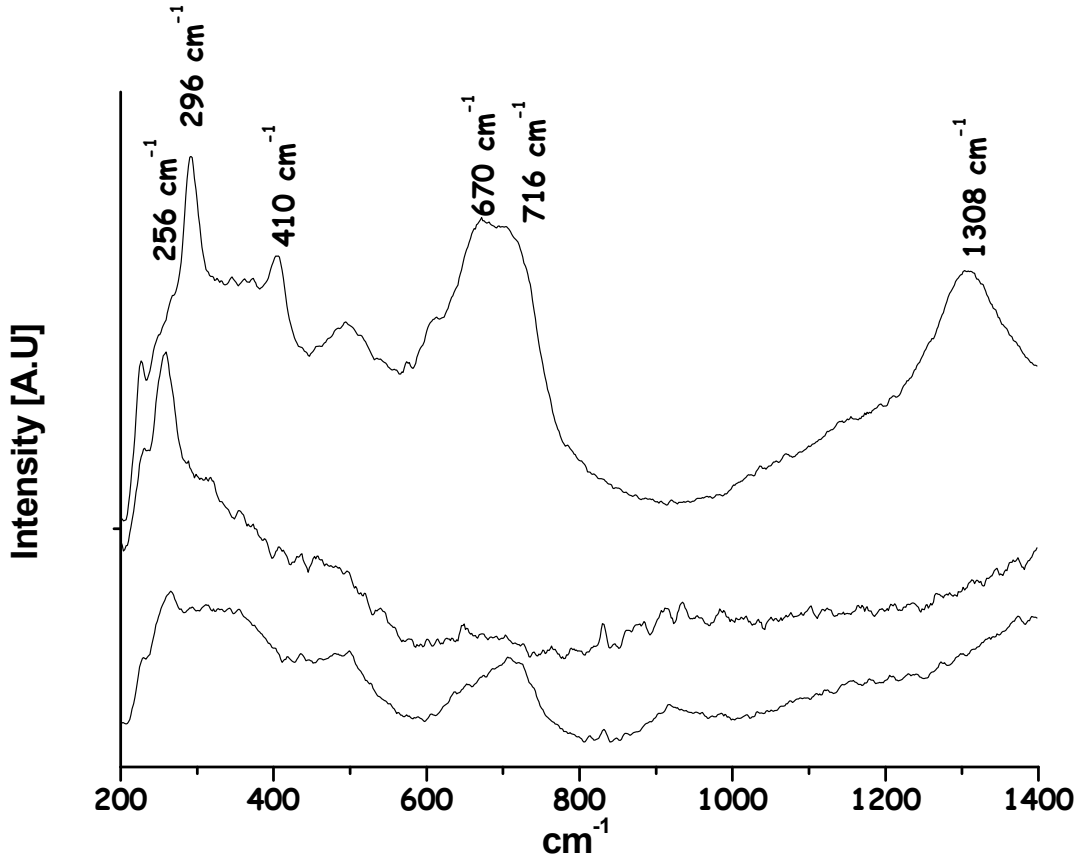

Figure 23: Raman spectra from three regions on sample N-250Se.

Raman spectroscopy of the HTP-samples also indicates the presence of the iron corrosion product magnetite (strong band at 670 cm^{-1}) and maghemite (broad band at ~716 cm^{-1}) on the samples. Evidence of a very heterogeneous spatial distribution of elemental Se (Figure 24 and 25) in samples HTP-250SeIV/420U, HTP-250SeVI/420U and HTP-250SeIV is given by the band at 236 cm^{-1} corresponding to the stretching mode of trigonal zero-valent Se [74].

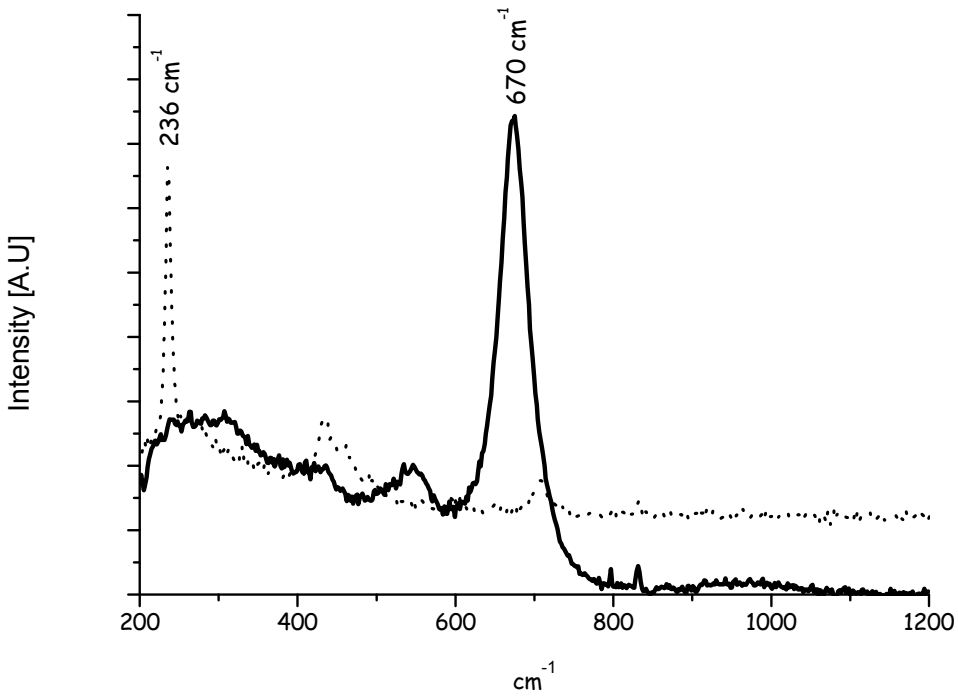

Figure 24: Two Raman spectra from sample HTP-250SeIV/420U.

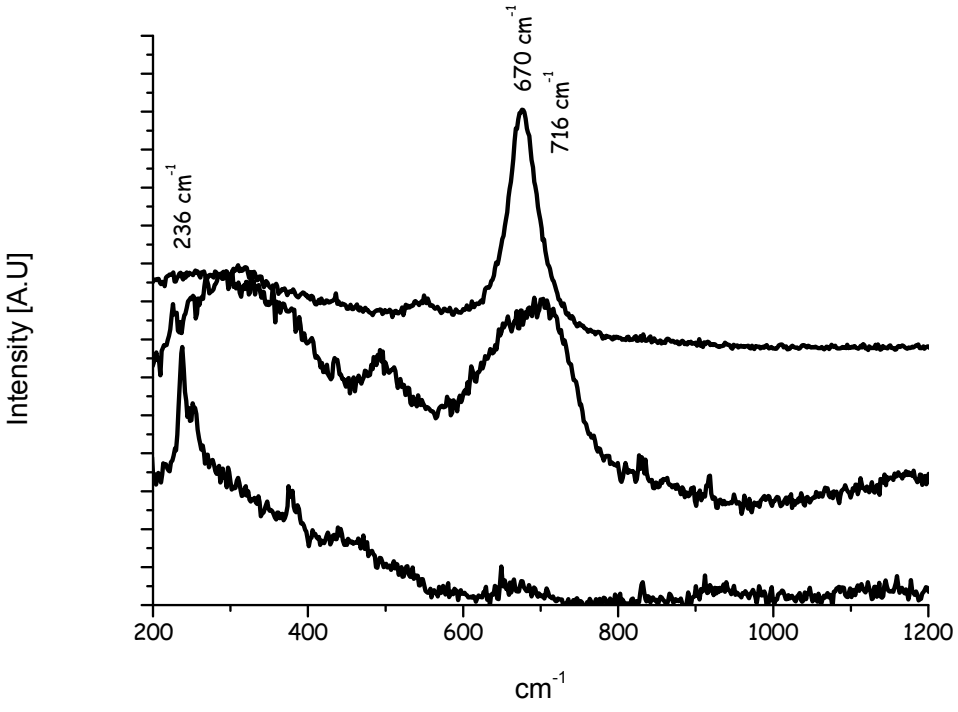

Figure 25: Three Raman spectra from sample HTP-250SeVI/420U.

The elemental spatial distribution of Fe, U and Se was investigated with SEM–EDS and microprobe fluorescence mapping. XRF and SEM–EDS scanning of sample N-250Se/420U revealed the presence of large amounts of Se and U. As can be seen in Figure. 26, the iron rich corrosion layer is extending a few µm from the cross section of the iron foil (20 µm initial foil thickness). Se rich regions appear to be associated with the edge of the iron corrosion front, mixed with uranium rich layers. The uranium layers on the top side of the foil extend over 100 µm from the iron foil and also appear to extend farther into the iron corrosion layer. The upper side in Figure. 26 with the thicker layers corresponds to the top side of the iron foil during the experiment. The foil was slightly bent to prevent the bottom side of the foil to be directly in contact with the vessel (not visible in Figure. 26). The conditions at the bottom side of the foil appear to have favored a sharper and thinner corrosion layer, particularly in the case of the thickness of the uranium layers. This could be due to the more limited exposure to the bulk solution or an effect of gravity given that the corrosion layers appeared to be loosely attached to the foil. As in the case of Raman spectroscopy, SEM–EDS analysis revealed a very heterogeneous Se distribution on the sample, with micrometer sized hotspots of up to 40 atom-% Se.

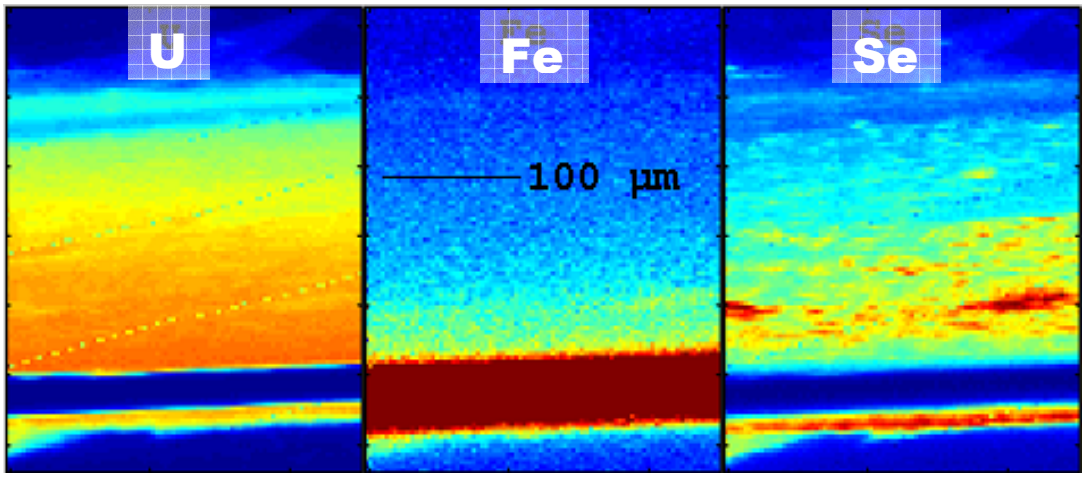

Figure 26. U, Fe and Se µ-XRF-map of a cross section of sample N-250SeVI/420U. Red corresponds to high and blue to low concentrations (The diagonal dots are an artifact from the mapping sequence).

In sample UP-250SeVI the uranium layers were more disrupted probably due to partial delamination of the thick layers during the long pre-corrosion time. Very little Se was observed on sample N-250SeVI with isolated small hotspots a few µm in size containing <1% Se. No Se was detected on sample UO_2–250SeVI.

SEM-EDS mapping of the corrosion products from sample HTP-250SeIV/420U gives an elemental distribution of ~40 %-mass uranium, with the remainder being mostly iron and oxygen as well as a few percent selenium and a smaller fraction of carbon and sodium. Mapping of corrosion products from sample HTP-250SeVI/420U gives very similar distributions with the possible difference that there is slightly less selenium. The uranium in the corrosion products from both samples appears to be rather homogenously distributed with no apparent hotspots and no indication of uranium rich crystals down to the resolution limit of the SEM-EDS (~0.1 µm). The Se in the studied samples is strongly associated with the acicular objects (Figures 27, 28, 29, 30). In sample HTP-250SeIV Se was also associated with spherical objects. Considering the Se Raman spectra of the samples and the documented formation of similar structures upon reduction of selenite they are most likely trigonal elemental Se crystals [111, 112].

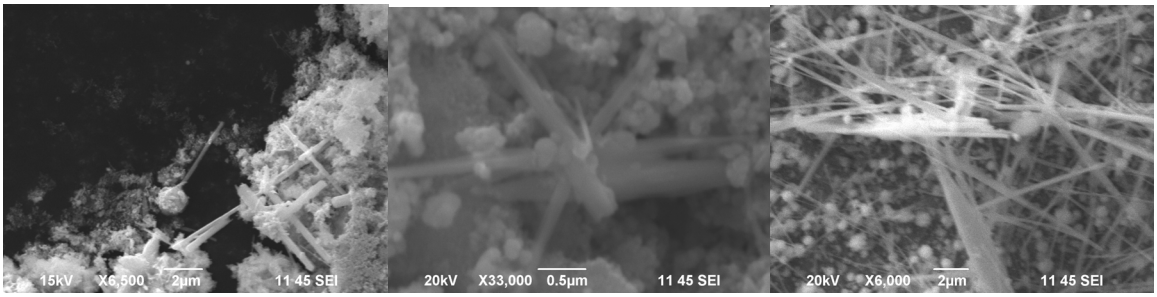

Figure 27: SEM image of corrosion products on samples HTP-250SeIV/420U (left), HTP-250SeVI/420U (middle) and HTP-250SeIV (right).

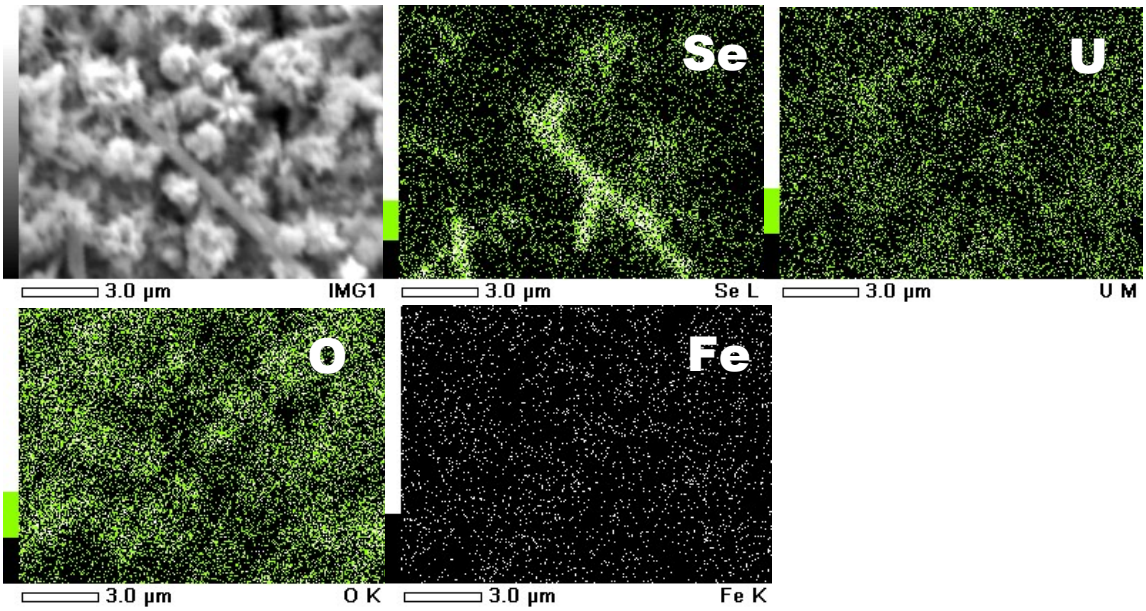

Figure 28: SEM-EDS mapping around acicular objects in corrosion products from sample HTP-250SeIV/420U.

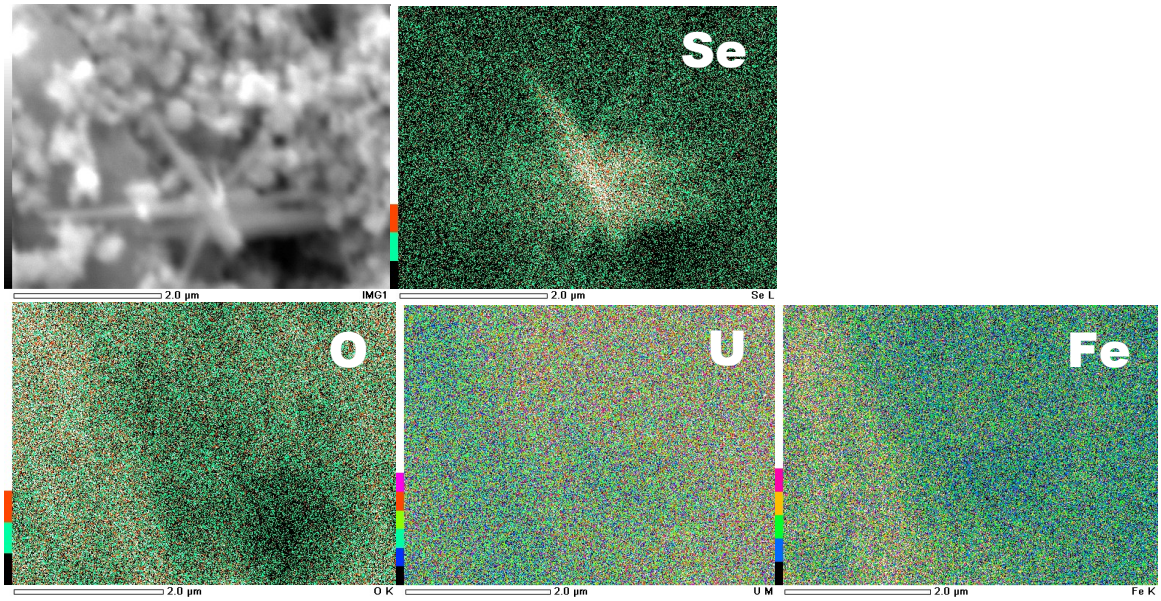

Figure 29: SEM-EDS mapping around acicular objects in corrosion products from sample HTP-250SeVI/420U.

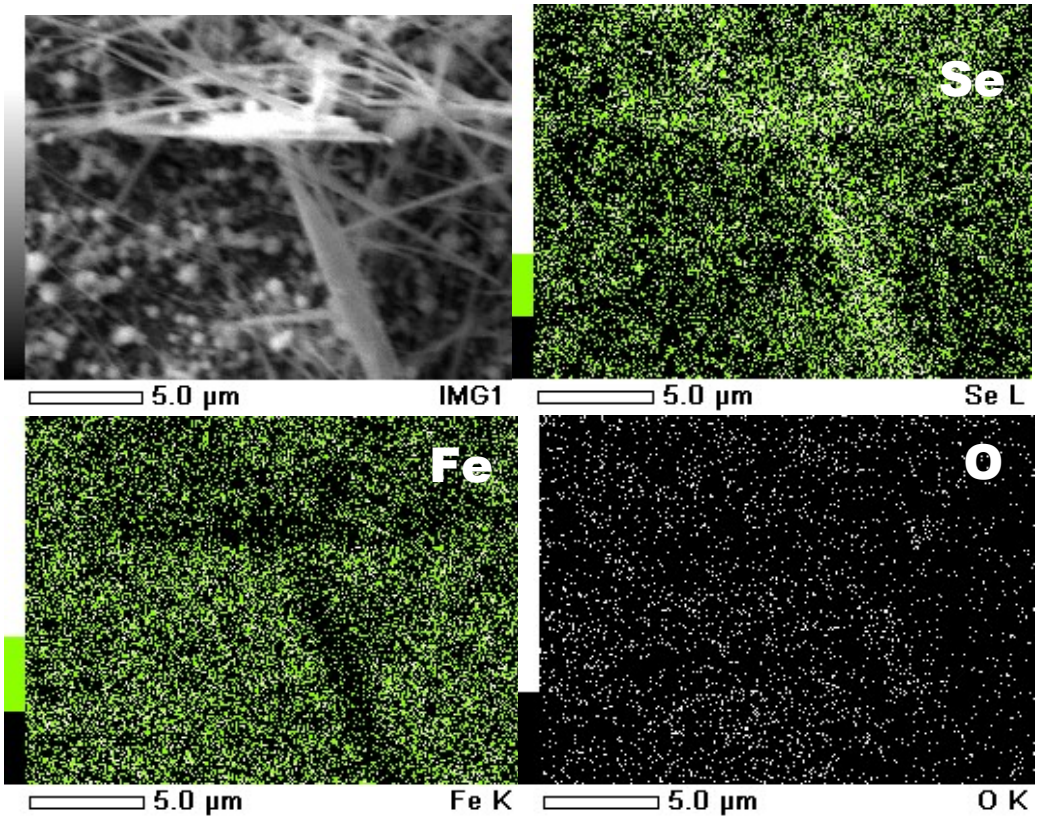

Figure 30: SEM-EDS mapping around acicular objects on sample HTP-250SeIV.

μ XANES (Micro X-ray Absorption Near Edge Structure) spectroscopy was employed to investigate the speciation of Se and U on the samples. Using the energy of the absorption edge at half-height of the normalized XANES for the Se(VI), (IV), (0) and ferroselite, Se(-I) reference materials resulted in a perfectly linear correlation ($R^2 = 0.9996$) of the edge energy to the oxidation state. Assigned edge energies of samples and references can be found in Table 8. XANES measurements were not performed on samples P250Se/420U and UO_2–250Se.

Table 8: Assigned edge energies based on half-height of the normalized spectra.

Se Sample	**Energy [eV]**
Sodiumselenate, Se(VI)	12660.6
Sodiumselenite, Se(IV)	12658.5
Gray Selenium, Se(0)	12653.9
Ferroselite, Se (-I)	12652.6
Dioctyldiselenide, Se(-I)	12654.3
HTP250SeVI/420U	12653.7
HTP250SeIV/420U	12653.9
N250SeVI/420U	12653.8
N250SeVI	12653.7
UP250SeVI	12653.9

U Sample	**Energy [eV]**
Uranylnitrate, U(VI)	17168.8
UO_2, U(IV)	17164.4
HTP250SeIV/420U	17164.4
HTP250SeVI/420U	17164.9
N250SeVI/420U	17164.4

Definite assignment of the oxidation state of reduced Se species from XANES spectra is however difficult as a non linear relationship was observed for the oxidation state and edge energy of the dioctyldiselenide Se(-I) reference. This phenomenon has been observed in several XAS studies of reduced selenium [93, 94, 113, 114]. The Se K edge has also been reported to be sensitive to varying degrees of crystallinity and different elemental allotropes [115]. The μ-XANES Se spectra of the samples do nevertheless have the same general features and closely matching edge energies regardless if the maximum of the first derivative of the edge, the edge maxima or the energy of the absorption edge at half-height of the normalized XANES is used to assign the edge energy.

The selenium on sample HTP-250SeVI/420U do exhibit an edge shift to slightly lower energy and a reduced edge height compared to the elemental Se and ferroselite references. These features have similarities to those observed and assigned to FeSe or other Se(-II) containing ironselenides [94, 103, 115]. Given the uncertainty in the exact Se speciation and the possible mixed Se oxidation state in the range from elemental Se to Se(-II) we conclude that the immobilized Se was reduced to Se(0) or lower oxidation states (based on the Se-XANES and Raman data). Representative selenium μ-XANES spectra from the samples and the bulk XANES spectra of reference compounds are presented in Figure. 31.

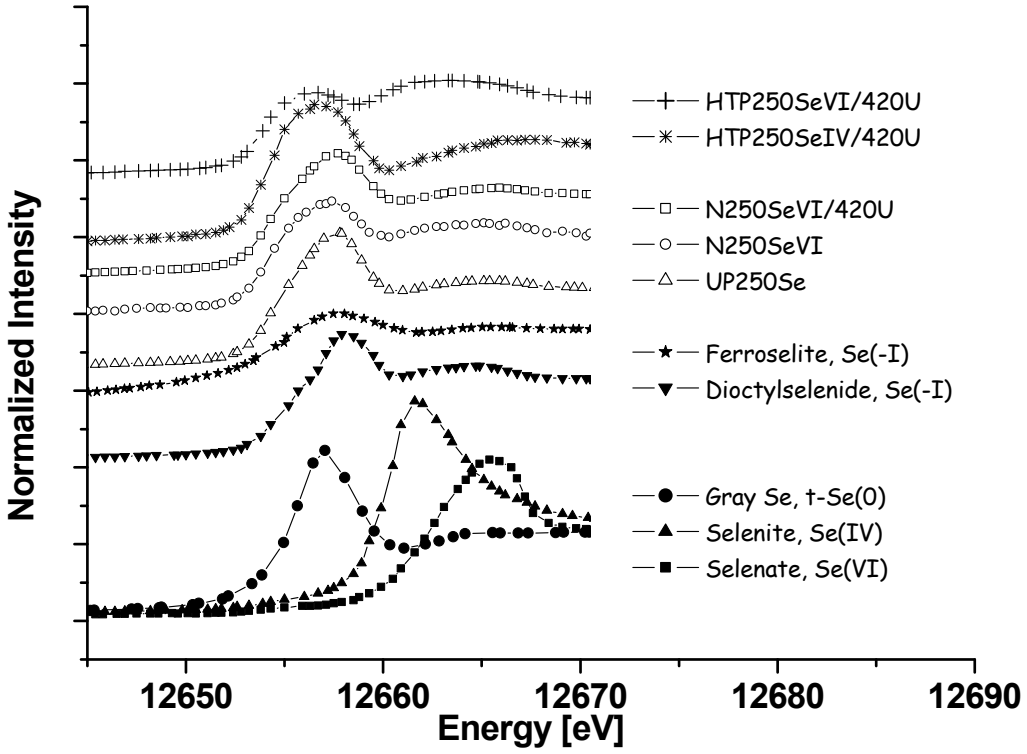

Figure 31: Selenium XANES spectra of investigated samples and reference compounds.

The oxidation state of the immobilized uranium on samples N-250Se/420U, 250SeIV/420U and 250SeVI/420U was investigated using μ-XANES (Figure 32). Linear combination fits, LCF of the experimental μ-XANES spectra with bulk XANES spectra of U(IV), UO_2 and U(VI), uranyl nitrate reference compounds revealed that the investigated uranium spots consisted of ~85-90% U(IV), i.e. the uranyl is largely reduced to U(IV) on the solid substrate. The LCF fits were processed using the Labview software package from beamline 10.3.2 [116]. No uranium species could however be detected by Raman spectroscopy despite the significant uranium content of up to ~40%-mass in the corrosion products (as determined by SEM-EDS). The absence of any discernable uranyl or cubic UO_2 bands in the Raman spectra combined with the U-XANES results of ~90 % U(IV) leads us to the conclusion that the uranium is likely present as amorphous or nanocrystalline UO_2.

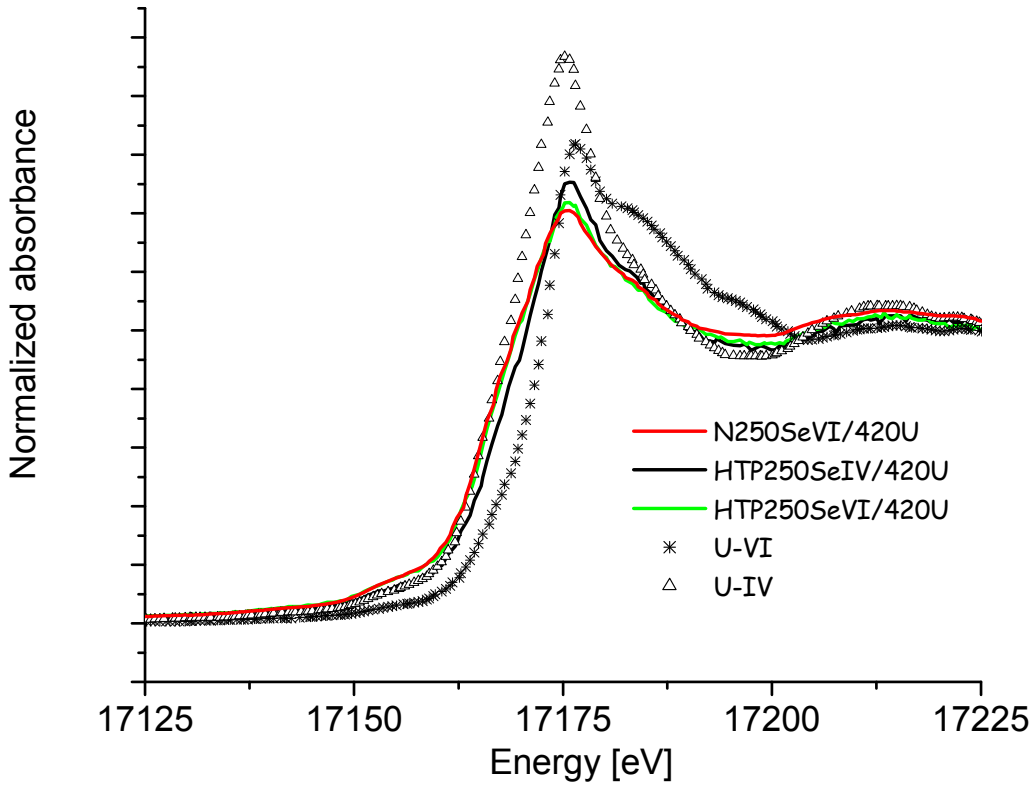

Figure 32: Uranium XANES spectra of investigated samples and reference compounds.

As was observed in samples N-250SeVI/420U, P-250SeVI/420U, HTP-250SeVI/420U and HTP-250SeIV/420U the presence of uranyl being removed significantly increased the rate of selenium immobilization. In the absence of uranyl the precorroded iron foil, HTP-250SeVI, with a magnetite layer appear to be inert towards selenate under the present conditions with no significant decrease in selenium concentration over 600 days despite the reducing conditions (redox potential ca -300 mV vs SHE). If reductive immobilization of selenate does not occur, this behavior is however not entirely unexpected given the small surface area and the limited selenate sorption capacity of magnetite at the pH ~8 [102]. The presence of uranyl and its subsequent immobilization by the corroded surfaces has a large impact on the reductive immobilization of dissolved selenate. The surface area does increase (by a factor of ~7 according to the BET measurement) and the pH is somewhat lower at ~7 when uranyl is present and being immobilized. But since no selenate is consumed in the sample without added uranyl the increased surface area from the reductive immobilization of uranyl does however not appear to fully explain the difference, particularily in the case of sample HTP-250SeIV/420U were all selenite is immobilized. For the precorroded samples the uranyl facilitated reduction of selenate is considerably slower than that of the selenite and appears to stop after immobilization of ~50% of the selenate in solution. Given the standard potential for reduction of selenate to selenite of 1.075 V [64] ($SeO_4^{2-} + 3H^+ + 2e^- \rightarrow HSeO_3^- + H_2O$), with a calculated equivalent standard potential of ~0.45 V (using Nernst equation) at pH 7 there appears to be no thermodynamic explanation for this difference in immobilization.

However, when intermediate Se(V) species are considered, data from the work of Kläning and Sehested [81] (and our own studies [117]) demonstrate that it takes either a two electron reductant or a stepwise reduction by a very strong one electron reductant to reduce selenate to selenite at the pH of the experiments (see Table 4 and 5 in the section covering papers I and II). There are no reports of hindering intermediates for the reduction of selenite to Se(0). Since oxidation of the magnetite layer would be expected to diminish its reductive capacity [118] the increased reductive removal of selenium due to the uranyl reduction and precipitation is somewhat unexpected. A hypothesis is that the magnetite film is incapable of reducing selenate but that the reduction of uranyl by the magnetite surface promotes its dissolution exposing the underlying iron, and thereby facilitating the reduction of selenate. Dissolved uranyl has been shown to be reduced by

magnetite [97], it has also been described that increasing the Fe(III) content of a magnetite film on iron promotes magnetite dissolution [119]. By the dissolution of the passive layer the selenate can contact the iron surface or a more reactive underlying Fe(II)/Fe(III) oxide. Several workers have reported on the reduction of selenite and selenate by Fe(II) oxidized from zero valent iron [89, 103] as well as by green rusts [90], which are mixed Fe(II)/(III) hydroxides [120]. Carbonate-green rusts in particular have been identified to form under conditions similar to those in the experiments with uranyl [95]. Since only approximately half of the selenate is removed (sample HTP-250SeVI/420U) before the surface appears to become passive again we conclude that the uranyl induced breach in the passive film is transient. This can be rationalized by the observations that magnetite is among the iron oxides formed when selenate is reduced by Fe(II)/(III) oxy/hydroxides [90, 121], so that the surface in the present case repassivates itself towards selenate immobilization by reformation of a magnetite layer. Maghemite, γ-Fe_2O_3, another candidate passifying oxide which can form from the topotactic oxidation of the Fe(II) in magnetite was also observed by Raman spectroscopy in sample HTP-250SeVI/420U (Figure 25). The magnetite layer is however not passive with regard to reduction of uranyl and selenite. The passivity of magnetite with regard to selenate reduction is in line with the recent XAS-study of Kvashnina et al [122] in which the selenium oxidation state was investigated on the surface of a polished and a precorroded iron surface after exposure to an anoxic selenate containing simulated groundwater solution. In that study the polished iron was found to reduce selenate to Se(-II), whereas the precorroded iron surface was only found to adsorb a very limited amount of selenate with no evidence of reduction. Although not mentioned in the paper, [122] the iron oxide in the precorroded sample was identified (by Raman spectroscopy) as being composed of magnetite.

In order to investigate the proposed mechanism for the magnetite film breaking effect of uranyl, additional experiments were performed in the absence of selenite or selenate. Iron powder, precorroded under the same conditions as the iron foils were used. Figure 33 shows the evolution of the corrosion products after addition of the uranyl solution (in 10 mM NaCl, 2 mM $NaHCO_3$, with ~10 times higher surface to volume ratio compared to the foil experiments with selenium).

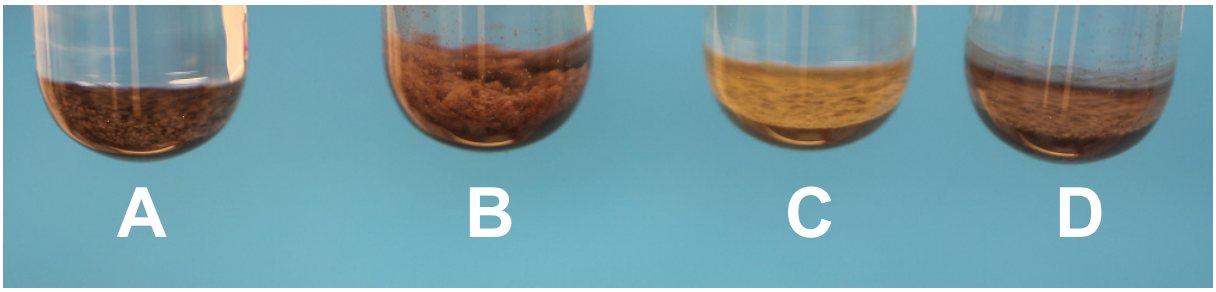

Figure 33: Photograph of the evolution of precorroded iron powder after the uranyl addition. A: Precorroded iron powder. B: After ~7 days. C: After ~21 days. D: ~90 days.

The uranyl dissappeared from solution within hours and within a few days a voluminous brownish precipitate formed on top of the corroded iron powder (represented by tube B, ~7 days in Figure 33). As time passed the corrosion products settled and shifted towards a brown/greenish colour (tube C, ~21 days, Figure 33). This layer slowly transformed over a few months into a black colour (tube D, ~90 days, Figure 33).

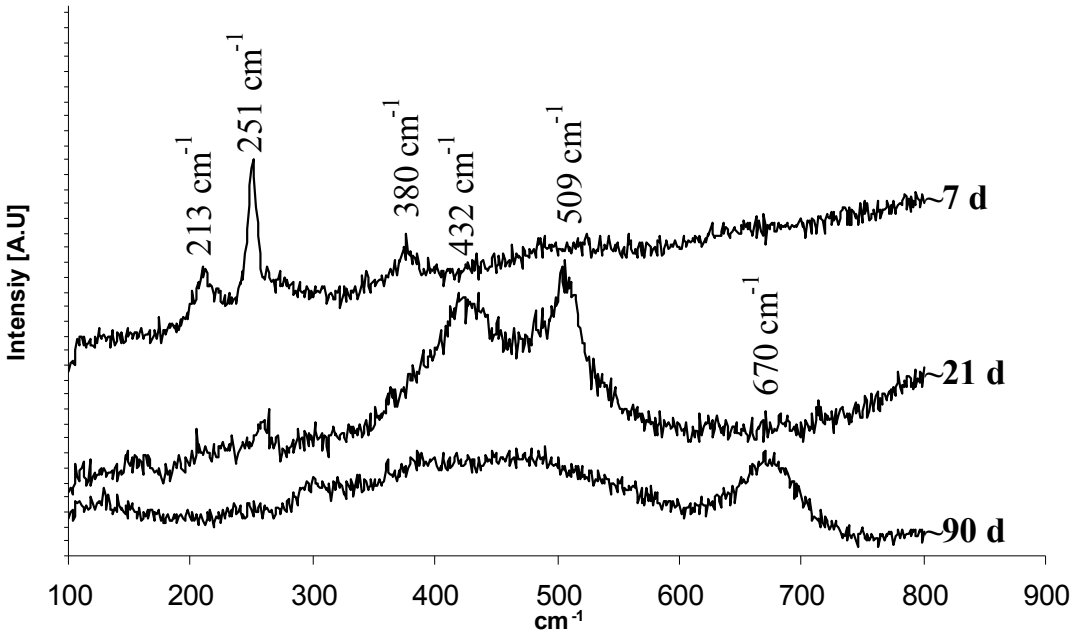

Figure 34: Raman spectra of the evolution of the corrosion products in Fig. 33.

As can be seen in Figure 34 the brownish corrosion product appearing after ~7 days was identified by Raman spectroscopy as lepidocrocite, γ-FeOOH based on the sharp strong band at 251 cm^{-1} and the broader bands at 213 cm^{-1} and 380 cm^{-1} [123]. The greenish product appearing after ~21 days was identified as a mixed Fe(II)/Fe(III) oxy-hydroxide based on the broad signals at ~432 cm^{-1} attributed to Fe(II)-OH stretching and that of Fe(III)-OH at ~509 cm^{-1} [124, 125]. Finally the black corrosion product forming after ~90 days was identified as magnetite by its band at 670 cm^{-1}.

Based on these observations we propose that the uranyl is rapidly adsorbed by the magnetite film and then reduced into UO_2 over the course of a few days. In doing so the magnetite layer is oxidized into a voluminous γ-FeOOH precipitate leading to break down of the magnetite film. This accelerates the corrosion of the underlying iron surface leading to an increase in Fe(II) content and the transition of the γ-FeOOH into a mixed Fe(II)/Fe(III) oxyhydroxide (green rust). The green rust does however appear to be a transient phase as magnetite is slowly reformed. These observations are in line with studies on the reaction of ferric oxyhydroxides (such as γ-FeOOH) and Fe(II) [126], including the observed formation of green rusts ([127], and references there in).

To summarize, selenate was found to be slowly reduced by iron surfaces whereas no reduction of selenate occurred on iron that was precorroded to give a several micro meter thick magnetite layer. Selenite was however slowly reduced by the precorroded iron surfaces. We propose that the barrier imposed by the reduction potential of intermediary Se(V) prevents reductive selenate immobilization by the magnetite surface. In the presence of uranyl also undergoing reductive immobilization the rate of selenite and selenate immobilization was considerably enhanced. In case of the magnetite covered iron surfaces we propose that the magnetite film is partially breached allowing the conduction of electrons or the outward diffusion of Fe(II) from the underlying iron, forming a more reactive Fe(II)/Fe(III) oxy-hydroxide enabling the selenate immobilization, predominantly to elemental Se.

The observations in this study show that reduction of dissolved uranyl by a corroding iron surface might greatly increase the reductive immobilization rate and capacity of the surface with regard to other dissolved contaminants such as selenate as well as selenite.

Remobilization of U and Se reductively immobilized on iron oxide surfaces (Paper V)

In a repository where UO_2-matrix dissolution is progressing, the release of radionuclides will cause radiolysis of the groundwater also in regions further away from the fuel surface. Hence, redox immobilized radionuclides could become re-mobilized as a result of radiation induced oxidative dissolution. We investigate the dynamics of re-mobilization of reductively immobilized U and Se using samples that were thoroughly characterized in two recent studies (paper III, IV). As described in [128, (paper III)] polished iron foils were reacted with uranyl and selenate under anoxic conditions. After the experiments described in [128] remaining reacted iron foils corresponding to the sample labelled N250Se/420U were employed for this study. The other sample used in this study, decribed in paper [129, (paper IV)] consisted of a pre-corroded iron foil with a magnetite corrosion layer. This sample was also reacted with uranyl and selenate and corresponds to the sample that was labelled 250SeVI/420U in [129]. In this thesis the sample is labelled HTP250SeVI/420U. For this study the remaining sample solutions over the foils were sampled, the solutions were then magnetically decanted leaving the foils and solid corrosion products. A new solution was then added (50 ml of 20 mM $NaHCO_3$) and sampled. After 49 hours hydrogen peroxide was added so that the solution now contained 100 mM H_2O_2 (50 ml volume) and sampling continued. The experiments were performed in a glove box (nitrogen, <0.1 ppm O_2) and all solutions were prepared from deoxygenated water. The samples were centrifuged and analyzed by ICP-OES. In order to assess the overall oxidation state of the uranium, carbonate leaching followed by hydrogen peroxide treatment was employed. At the higher bicarbonate concentration (20 mM $NaHCO_3$) adsorbed uranyl was expected to dissolve. The maximum uranium concentration prior to addition of H_2O_2 was reached within one hour after which the uranium concentration slowly began to decrease again. Hydrogen peroxide was then added to the solution. The H_2O_2 (100 mM) in combination with the carbonate will oxidize and dissolve the remaining U(IV) at the surfaces.

Sample N250Se/420U had less than 0.05 μM of either Se or U remaining in the original solution from the experiments described in [128] (less than the detection limit corresponding to <10 ppb in the sample prior to analysis dilution). In sample HTP250SeVI/420U a significant amount of Se ~98 μM and ~0.1 μM of U remained in

solution from the experiments described in [129]. Since the solutions were exchanged a large amount of Se was thus removed from the experiment with the discarded original solution for sample HTP250SeVI/420U. The solutions used in the immobilization experiments contained 0.25 mM SeO_4^{2-} and 0.42 mM UO_2^{2+}. After immobilization, >99 % of the solutes had been removed from the solution for sample N250SeVI/420U and the overall relative composition of the deposit is expected to be identical to the original composition of the solution. In the case of sample HTP250SeVI/420U >99% of the uranium had also been immobilized, but a large amount of Se remained in solution (~98 µM with ~25ml remaining out of 250 µM and 50ml at the start) and was thus removed prior to these experiments.

Addition of HCO_3^- to the immobilized samples immersed in water is expected to solubilize U(VI) and addition of H_2O_2 is expected to oxidize U(IV) to U(VI) and thereby solubilize all of the uranium. Upon addition of HCO_3^- a rapid but transient increase in uranium concentration could be observed (Figure 35).

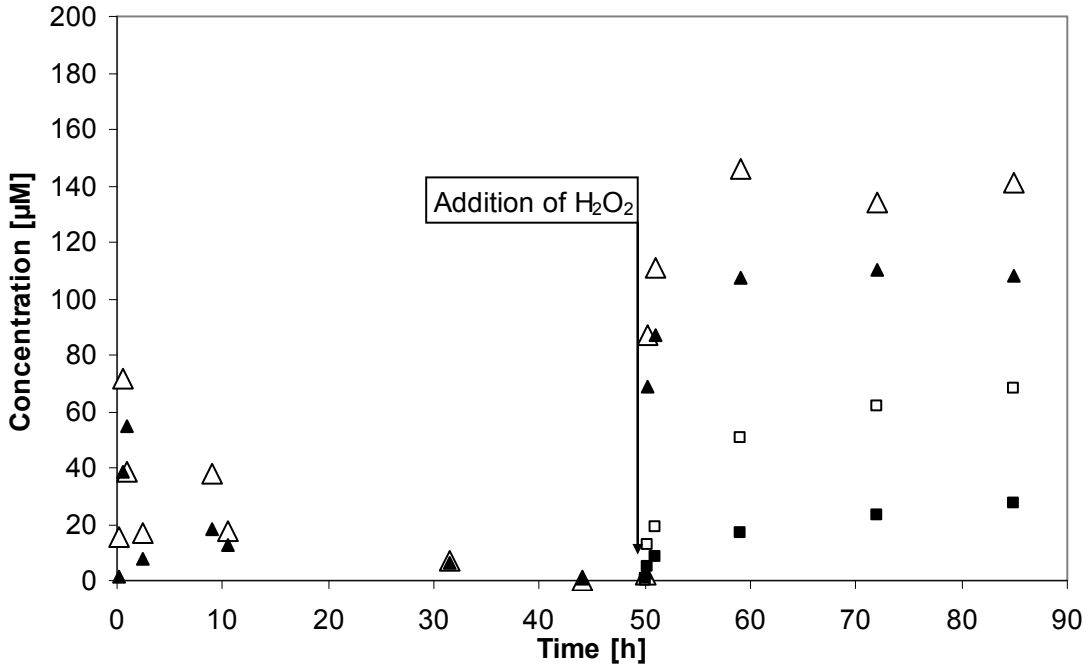

Figure 35: U in sample N250SeVI/420U (Δ), U in sample HTP250SeVI/420U (▲), Se in sample N250SeVI/420U (□), Se in sample HTP250SeVI/420U (■).

The rationale for the transient uranium concentration peak is most probably that the samples contained loosely bound UO_2 particles that were detached from the surface upon addition of the new solution. These particles settled after some time.

In Figure 36 the uranium and selenium concentrations are plotted for a longer time scale after addition of H_2O_2 to the solutions.

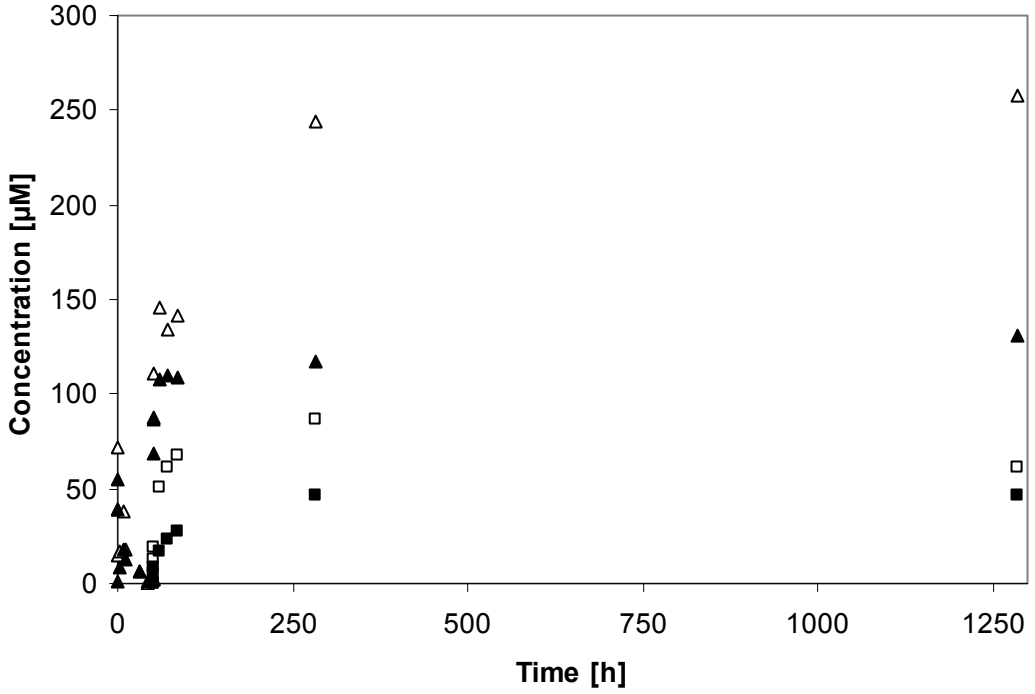

Figure 36: U in sample N250SeVI/420U (Δ), U in sample HTP250SeVI/420U (▲), Se in sample N250SeVI/420U (□), Se in sample HTP250SeVI/420U (■).

As can be seen, the concentration of uranium increases with time. The initial rate of uranium dissolution is ca 10^{-8} M s^{-1}. From the previously determined rate constant for the reaction between H_2O_2 and UO_2 (7.3 x 10^{-8} m s^{-1} [130]), the initial concentration of H_2O_2 (0.1 mol dm^{-3}), the estimated geometrical surface area of UO_2 (4 cm^2) and the surface composition we can estimate the rate of UO_2 oxidation in these experiments to be of the same order of magnitude. A more precise estimation is not possible since the UO_2 particle size at the surface is not known. The particle size has been shown to influence the rate constant for oxidation of UO_2 by H_2O_2 significantly [131].

Upon inspection of the data displayed in Figure 36 it also becomes obvious that the Se/U ratio increases with leaching time approaching the overall original composition of the immobilized surface. Hence, oxidative dissolution of the immobilized U and Se is not

congruent. This could be attributed to the heterogeneous nature of the surface deposit but also to the difference in redox reactivity between the two elements. It should be stressed that while oxidative dissolution of UO_2 only requires transfer of two electrons, oxidative dissolution of Se(0) requires transfer of at least four electrons. Hence, at least two equivalents of H_2O_2 is needed for the latter process. The initial rate of Se release is in the order of 10^{-9} M s^{-1} which is one order of magnitude lower than the initial rate of U release. The somewhat delayed release of Se indicates that oxidation is a prerequisite for re-mobilization. Iodometric titrations at the end of the experiments do not reveal any remaining oxidant in solution (capable of oxidizing I^-). Since both H_2O_2 and Se(IV) would have oxidized I^- to I_3^-, the majority of the remobilized selenium should thus be Se(VI).

It is also interesting to note that the iron oxide surface exposed to the solution after oxidative removal of the immobilized Se and U appears to be unreactive towards U in solution, although the Se concentration in solution does appear to decrease slightly over longer time scales. Consequently, the oxidative remobilization process has also affected the iron oxide. As demonstrated above, oxidative re-mobilization of reductively immobilized redox sensitive radionuclides is a process of potential impact in a deep geological repository for spent nuclear fuel.

Conclusions

Selenite was found to adsorb on Pd(s) (in simulated groundwater 10 mM NaCl, 10 mM $NaHCO_3$) with a site density of ~10 selenite molecules per nm^2. Under hydrogen and Pd(s) selenite was reduced to elemental colloidal Se. Pd doped UO_2 was found to increase the rate of selenite reduction by about two orders of magnitude with respect to the Pd surface, indicating that UO_2 can operate as an efficient co-catalyst to Pd. UO_2 alone did not appear to have any significant adsorption or reduction capacity towards selenite or selenate under hydrogen. No adsorption or reduction of selenate appears to occur for the Pd/hydrogen system.

Iron and iron covered by corrosion products were found to have a large capacity to immobilize and reduce dissolved redox sensitive species, such as uranyl and selenite, under anoxic conditions, despite the unfavorably low surface to volume ratios of the experiments in this thesis. This indicates that the iron in the canister material can have a very large impact on the inhibition of release of radionuclides after failure of the canister (water intrusion). Furthermore, the reduction of dissolved uranyl into UO_2 by the corroding iron surfaces, was found to significantly increase the immobilization rate of selenite as well as selenate. The uranyl was found to transiently transform the outer iron oxide layers on the iron, forming a reactive mixed Fe(II)/Fe(III) oxyhydroxide (Green rust). The speciation of escaping redox sensitive radionuclides of interest, such as Se^{79}, is of great significance for the effectiveness of the immobilization in both the studied Pd/H_2 system and for the iron/iron-hydroxy-oxides, as was demonstrated by the, in some instances dramatic, difference in degree of removal between selenate and selenite. A radiation chemical experiment was also performed, confirming the one electron reduction barrier of selenate as an important factor in systems where selenate reduction would be thermodynamically favorable.

A large degree of the immobilization processes studied in the thesis depends on reducing conditions, some requiring the evolution of hydrogen gas. On the other hand, if oxidizing conditions should occur (such as if hydrogen peroxide formed by radiolysis would come to at least locally set the redox conditions), it could cause remobilization or seriously diminish the radionuclide retention capacity of the iron canister material.

Outlook

Palladium does not appear to catalyse the reduction of selenate under hydrogen atmosphere. It would, however, be most interesting to examine if the noble metal particles present in spent nuclear fuel might catalyse selenate reduction under hydrogen atmosphere. Since the noble metal particles are an alloy of elements, they might operate in a way similar to that of bimetallic catalysts, and thus facilitate the two-electron transfer reduction that appears to hinder the reduction of selenate. Such information would definitely be helpful in assessing the catalytic properties of spent nuclear fuel.

It would also be intriguing to perform further investigations on the synergistic effect of uranyl reduction on the ability of corroding iron to reductively remove selenium oxyanions. Particularly it would be valuable to confirm the mechanism, and to examine if the effect is also observable for other redox sensitive contaminants.

Acknowledgments

Firstly, I would like to thank Professor Mats Jonsson, my supervisor, for his support, encouragement and for enduring with me. I also extend my thanks to Professor Emeritus Trygve E. Eriksen for his most helpful comments on the thesis.

The Swedish Nuclear Fuel and Waste Management Co., SKB is gratefully acknowledged for financial support. I especially wish to thank Professor Kastriot Spahiu for sharing his experience and providing appreciated criticism.

I thank past and present colleagues at the divisions of Nuclear Chemistry, and Inorganic Chemistry at KTH. In particular I would like to thank Dr Mats Jansson, for his friendship, and for as always offering his assistance whenever a problem presented itself, Professor Johan Lind and Professor Gábor Merényi for most valued advice, and Martin Trummer for a good collaboration.

I would also like to thank the colleagues at the hot cell laboratory at Studsvik Nuclear AB, for sharing their hands-on knowledge on nuclear fuel; Dr Ella Ekeroth for the time at Nuclear Chemistry and for providing a challenging start for me in Studsvik; Dr Daqing Cui, for his support and advice on everything from cooking to noble metal inclusions – although I am uncertain whether I should thank him for introducing me to the elusive green rust at the beginning of my Ph.D. studies – and Carolina Losin, for encouraging me to carry on and finalise this thesis.

I would also like to thank Dr Rainer Dähn, Dr André Scheidegger and Dr Erich Wieland from the Paul Scherrer Institut (PSI); for teaching me the basics of XAS, their valuable advice, and the beam time at ALS in Berkeley, USA and SLS at PSI, Switzerland.

Last but certainly not least I thank my family for their love and for backing me, in particular my darling Camilla for the endless support and little Alvin for being such a joy.

References

[1] R.L. Segall, R.S.C. Smart, J. Nowotny, Surface and Near-Surface Chemistry of Oxide Materials, Elsevier Science Publishers B.V., Amsterdam, Netherlands, 1988 527.

[2] D. Rai, A.R. Felmy, J.L. Ryan, Inorg. Chem. 29 (1990) 260.

[3] I. Casas, J. de Pablo, J. Giménez, M.E. Torrero, J. Bruno, E. Cera, R.J. Finch, R.C. Ewing, Geochim. Cosmochim. Acta 62 (1998) 2223.

[4] J.W.T. Spinks, R.J. Woods, An Introduction to Radiation Chemistry, John Wiley, New York (1964) 477.

[5] O. Roth, M. Jonsson, Cent. Eur. J. Chem. 6 (2008) 1.

[6] E. Ekeroth, O. Roth, M. Jonsson, J. Nucl. Mater. 355 (2006) 38.

[7] I. Grenthe, F. Diego, F. Salvatore, G. Riccio, J. Chem. Soc. Dalton Trans. 11 (1984) 2439.

[8] J. de Pablo, I. Casas, J. Giménez, M. Molera, M. Rovira, L. Duro, J. Bruno, Geochim. Cosmochim. Acta 63 (1999) 3097.

[9] D.E. Grandstaff, Econ. Geol. 71 (1976) 1493.

[10] W. J. Gray, J.C. Tait, S.A. Steward, D.W. Shoesmith, High Level Radioactive Waste Management, V Annual International Conference, La Grange Park, IL, (1994) 2597.

[11] E.M. Pierce, J.P. Icenhower, R.J. Serne, J.G. Catalano, J. Nucl. Mater. 345 (2005) 206.

[12] L. Johnson, C. Ferry, C. Poinssot and P. Lovera, J. Nucl. Mater. 346 (2005) 56.

[13] P. Carbol, J. Cobos-Sabathe, J.-P. Glatz, C. Ronchi, V. Rondinella, D.H. Wegen, T. Valiente, SKB Tech. Rep. TR-05-09 (2005).

[14] T.E. Eriksen, M. Jonsson, SKB Tech. Rep. TR-07-06 (2007).

[15] K. Spahiu, J. Devoy, D. Cui, M. Lundström, Radiochim. Acta 92 (2004) 597.

[16] S. Rollin, K. Spahiu, U.-B. Eklund, J. Nucl. Mater. 297 (2001) 231.

[17] P. Carbol, P. Fors, T. Gouder, K. Spahiu, Geochim. Cosmochim. Acta 73 (2009) 4366.

[18] D. Cui, J. Low, C.J. Sjöstedt, K. Spahiu, Radiochim. Acta 92 (2004) 551.

[19] M. Jonsson, F. Nielsen, O. Roth, E. Ekeroth, S. Nilsson, M.M. Hossain, Environ. Sci. Technol. 41 (2007) 7087.

[20] N.R. Smart, D.J. Blackwood, L. Werme, Corrosion 58 (2002) 627.

[21] B. Bonin, M. Colin, A. Dutfoy, J. Nucl. Mater. 281 (2000) 1.

[22] ANDRA 2005, Dossier 2005 Argile: Safety Evaluation of a Geological Repository.

[23] Nagra, 2002. Project Opalinus clay, demonstration of disposal feasibility for spent fuel, vitrified high-level waste and long-lived intermediate-level waste: Safety Report, Technical report, 02–05.

[24] M. Navarro-Alarcon, C. Cabrera-Vique, Sci. Total Environ. 400 (2008) 115.

[25] A. Fernandez-Martinez, L. Charlet, Rev. Environ. Sci. Biotechnol. 8 (2009) 81.

[26] M. Lenz, P.N.L. Lens, Sci. Total Environ. 12 (2009) 3620.

[27] K.S. Dhillon, S.K. Dhillon, Adv. Agron. 79 (2003) 119.

[28] J.R. Muscatello, A.M. Belknap, D.M. Janz, Environ. Pollut. 156 (2008) 387.

[29] A.D. Lemly, Ecotoxicol. Environ. Saf. 59 (2004) 44.

[30] H. Rune, SKB Report, R-99-74 (2000).

[31] L.E. Glendenin, Report MDDC 1694-C (1948).

[32] G.W. Parker, G.E. Creek, G.M. Hebert, P.W. Lantz, W.J. Martin, Report ORNL-499 (1949).

[33] B. Singh, O.W. Hermann, Nucl. Data Sheets 70 (1993) 452.

[34] Ch. Zhou, Z. Wu, Nucl. Sci. Tech. 17 (2006) 21.

[35] R. Yu, J. Guo, A. Cui, P. Tang, D. Li and D. Liu, J. Radioanal. Nucl. Chem. Art. 196 (1995) 165.

[36] S. Jiang, J. Guo, S. Jiang, Ch. Li, A. Cui, M. He, S. Wu, S. Li, Nucl. Instrum. Methods Phys. Res., Sect B 123 (1997) 405.

[37] M. He, S. Jiang, S. Jiang, Qu. Chen, J. Qin, S. Wu, Y. Dong, Z. Zhao, Nucl. Instrum. Methods Phys. Res. B 172 (2000) 177.

[38] S. Jiang, M. He, L. Diao, J. Guo, S. Wu, Chin. Phys. Lett. 18 (2001) 746.

[39] M. He, S. Jiang, S. Jiang, L. Diao, S. Wu, Ch. Li, Nucl. Instrum. Methods Phys. Res. Sect. B 194 (2002) 398.

[40] Ph. Bienvenu, Ph. Cassette, G. Andreoletti, M. Bé, J. Comte, M. Lépy, Appl. Radiat. Isot. 65 (2007) 355.

[41] G. Jörg, R. Bühnemann, S. Hollas, N. Kivel, K. Kossert, S. Van Winckel, C. L. V. Gostomski, Appl. Radiat. Isot. 68 (2010) 2339.

[42] S. Imoto, J. Nucl. Mater. 140 (1986) 19.

[43] A.L. Nichols, D.L. Aldama, M. Verpelli, Handbook of Nuclear Data for Safeguards. IAEA INDC(NDS)-0534 (2008).

[44] R.A. Dewberry, J.D. Leyba, W.T. Boyce, J. Radioanal. Nucl. Chem, 3 (2000) 491.

[45] J. Comte, P. Bienvenu, E. Brochard, J-M. Fernandez, G. Andreoletti, J. Anal. At. Spectrom, 18 (2003) 702.

[46] R. Brennetot, L. Pierry, T. Atamyan, G. Favre, D. Vailhen, J. Anal. At. Spectrom. 23 (2008) 1350.

[47] C.N. Wilson, HEDL-TME 85-22 UC-70 (1987), Westinghouse Hanford Company.

[48] H. Kleykamp, J. Nucl. Mater, 2-3, (1985) 221.

[49] G. Chattopadhyay, J.M. Juneja, J. Nucl. Mater, 1-2, (1993) 10.

[50] W.H. Hocking, A.M. Duclos, L.H. Johnson, J. Nucl. Mater, 1 (1994) 1.

[51] D. Cui, J. Low, C.J. Sjöstedt, K. Spahiu, Radiochim. Acta 92 (2004) 551.

[52] M. Uno, H. Kinoshita, T. Nakai, M. Horie, Technology Reports of the Osaka University, 48 (1998) 181.

[53] G. Kosec, L. Kosec, I. Anzel, V. Gontarev, B. Kosec, M, Bizjak, Metalurgija 44 (2004) 37

[54] L. H. Johnson, D. F. McGinnes, Technical Report NAGRA TR 02-07.

[55] R. Bros, H. Hidaka, G. Kamei, T. Ohnuki, Appl. Geochem, 12 (2003) 1807.

[56] H. Hidaka, P. Holliger, F. Gauthier-Lafay, Chem. Geol, 155 (1999) 323.

[57] L. Auqué, M.J. Gimeno, J. Gómez, A.C. Nilsson, Appl. Geochem. 23 (2008) 1820.

[58] C. Bruggeman, J. Vancluysen, A. Maes, Radiochim. Acta. 90 (2002) 629.

[59] R. Doi, H. Tachikawa, M. Yui, J. Nucl. Sci. Technol. 47 (2010) 278.

[60] F. Chen, P.C. Burns, R.C. Ewing, J. Nucl. Mater. 1 (1999) 81.

[61] K.F. Hayes, A.L. Roe, G.E. Brown, K.O. Hodgson, J.O. Leckie, G.A. Parks, Science 238 (1987) 783.

[62] H. Sato, S. Miyamoto, Appl. Clay Sci.1-4 (2004) 47.

[63] T. Beauwens, P. Cannière, H. Moors, L. Wang, N. Maes, Eng. Geol. 77 (2005) 285.

[64] F. Séby, M. Potin-Gautier, E. Giffaut, G. Borge, O.F.X. Donard, Chem. Geol. 171 (2001) 173.

[65] M. Trummer, S. Nilsson, M. Jonsson, J. Nucl. Mater. 378 (2008) 55

[66] A.M. Scheidegger, D. Grolimund, M. Harfouche, M. Willimann, B. Meyer, R. Dähn, D. Gavillet, M. Nicolet, P. Heimgartner, NEA Publication No. 6046 (2006) 81.

[67] L. Syper, J. Mlochowski, Synthesis 5 (1984) 439.

[68] T. Ressler, J. Synchrotron Radiat. 5 (1998) 118.

[69] M.E. Broczkowski, J.J. Noel, D.W. Shoesmith, J. Nucl. Mater. 346 (2005) 16.

[70] D. Cui, J. Low, V.V. Rondinella, K. Spahui, Appl. Catal. B Environ. 94 (2010) 173.

[71] P. Mendes, Comput. Appl. Biosci. 9 (1993) 563.

[72] A.A. Serov, S.Y. Cho, S. Han, M. Min, G. Chai, K.H. Nam, C. Kwak, Electrochem. Commun. 9 (2007) 2041.

[73] C. Wei, N. Myung, K. Rajeshwar, J. Electroanal. Chem. 375 (1994) 109.

[74] V.V. Poborchii, A.V. Kolobov, K. Tanaka, Appl. Phys. Lett. 72 (1998) 1167.

[75] S.N. Yannopoulos, K.S. Andrikospoulos, J. Chem. Phys. 121 (2004) 4747.

[76] S. Nilsson, M. Jonsson, J. Nucl. Mater. 372 (2008) 160.

[77] N. Munakata, M. Reinhard, Appl. Catal. B: Environ. 75 (2007) 1.

[78] S.I. Fukuzawa, T. Fujinami, S. Sakai, Chem. Lett. 19 (1990) 927.

[79] M. Trummer, O. Roth, M. Jonsson, J. Nucl. Mater. 383 (2008) 226.

[80] D. Cui, A. Puranen, J. Devoy, A. Scheidegger, X.O. Leupin, P. Wersin, R. Gens, K. Spahiu, J. Radioanal. Nucl. Chem. 282 (2009) 349.

[81] U.K. Kläning, K. Sehested, J. Phys. Chem. 90 (1986) 5460.

[82] J. Lilie, G. Beck, A, Henglein, Ber. Bunsen-Ges. Phys. Chem. 75 (1971) 458.

[83] K.L. Nuttall, F. Allen, Inorg. Chim. Acta 92 (1984) 33.

[84] A. Goldbach, J. Johnson, D. Meisel, L.A. Curtiss, M.L. Saboungi, J. Am. Chem. Soc. 121 (1999) 4461.

[85] K.L. Nuttall, A.F. Allen, Inorg. Chim. Acta 91 (1984) 243.

[86] K.L. Nuttall, F. Allen, Inorg. Chim. Acta 89 (1984) 199.

[87] SKB Technical Report, TR-06-22 (2006).

[88] A.P. Murphy, Ind. Eng. Chem. Res. 27 (1988) 187.

[89] Y. Zhang, J. Wang, C. Amrhein, W.T. Frankenberger Jr., J. Environ. Qual. 34 (2005) 487.

[90] S.C.B. Myneni, T.K. Tokunaga, G.E. Brown, Science 278 (1997) 1106.

[91] S.R. Qiu, H.F. Lai, M.J. Roberson, M.L. Hunt, C. Amrhein, L.C. Giancarlo, G.W. Flynn, J.A. Yarmoff, Langmuir 16 (2000) 2230.

[92] A.M. Scheidegger, D. Grolimund, D. Cui, J. Devoy, K. Spahiu, P. Wersin, I. Bonhoure, M. Janousch, J. Phys. IV: Proc. 104 (2003) 417.

[93] A.C. Scheinost, R. Kirsch, D. Banerjee, A. Fernandez-Martinez, H. Zaenker, H. Funke, L. Charlet, J. Contam. Hydrol. 102 (2008) 228.

[94] A.C. Scheinost, L. Charlet, Environ. Sci. Technol. 42 (2008) 1984.

[95] M. Wazne, G.P. Korfiatis, X. Meng, Environ. Sci. Technol. 37 (2003) 3619.

[96] O. Riba, T.B. Scott, K.V. Ragnarsdottir, G.C. Allen, Geochim. Cosmochim. Acta 72 (2008) 4047.

[97] D. Cui, K. Spahiu, Radiochim. Acta 90 (2002) 623.

[98] T.B. Scott, G.C. Allen, P.J. Heard, M.G. Randell, Geochim. Cosmochim. Acta 69 (2005) 5639.

[99] E.J. O'Loughlin, S.D. Kelly, R.E. Cook, R. Csencsits, K.M. Kemner, Environ. Sci. Technol. 37 (2003) 721.

[100] N.R. Smart, D.J Blackwood, L. Werme, SKB-Technical Report TR-01-22 (2001).

[101] K. Ritter, M.S. Odziemkowski, R.W. Gillham, J. Contam. Hydrol. 55 (2002) 87.

[102] M. Martínez, J. Giménez, J. de Pablo, M. Rovira, L. Duro, Appl. Surf. Sci. 252(2006) 3767.

[103] R. López de Arroyabe Loyo, S.I. Nikitenko, A.C. Scheinost, M. Simonoff, Environ. Sci. Technol. 42 (2008) 2451.

[104] S.J. Morrison, D.R. Metzler, B.P. Dwyer, J. Contam. Hydrol. 56 (2002) 99.

[105] J.R. Muscatello, D.M. Janz, Sci. Total Environ. 407 (2009) 1318.

[106] D. Nafts, S. Morisson, C. Fuller, J. Davies, Handbok of Groundwater Remediation Using Permeable Reactive Barries (2002).

[107] D.L.A. De Faria, S. Venâncio Silva, M.T. De Oliveira, J. Raman Spectrosc. 28 (1997) 873.

[108] D. Manara, B. Renker, J. Nucl. Mater. 321 (2003) 233.

[109] V. Poborchii, A. Kolobov, H. Oyanagi, S. Romanov, K. Tanaka, Nanostruct. Mater. 10 (1998) 427.

[110] Q. Li, V. Wing-Wah Yam, Chem. Commun. (2006) 1006.

[111] C. An, S. Wang, Mater. Chem. Phys. 101 (2007) 357.

[112] F. Du, H. Wang, J. Mater. Sci. 42 (2007) 9476.

[113] A. Ryser, D. Strawn, M. Marcus, J. Johnson-Maynard, M. Gunter, G. Möller, Geochem. Trans. 6 (2005) 1.

[114] M. Lenz, E.D. Van Hullenbusch, F. Farges, S. Nikitenko, C.N. Borca, P.N.L. Lens, Environ. Sci. Technol. 42 (2008) 7587.

[115] I.J. Pickering, G.E. Brown, T.K. Tokunaga, Environ. Sci. Technol. 29 (1995) 2456.

[116] M. Marcus, A.A. MacDowell, R. Celestre, A. Manceau, T. Miller, H.A. Padmore, R.E. Sublett, J. Synchrotron. Radiat. 11 (2004) 239.

[117] A. Puranen, M. Jansson, M. Jonsson, J. Contam. Hydrol. 116 (2010) 16.

[118] C.A. Gorski, J.T. Nurmi, P.G. Tratnyek, T.B. Hofstetter, M.M. Scherer, Environ. Sci. Technol. 44 (2010) 55.

[119] W.S. Li, J.S. Luo, Int. J. Electrochem. Sci. 2 (2007) 627.

[120] I.R. McGill, B. McEnaney, D.C. Smith, Nature 259 (1976) 200.

[121] H. Hayashi, K. Kanie, K. Shinoda, A. Muramatsu, S. Suzuki, H. Sasaki, Chemosphere 76 (2009) 638.

[122] K.O. Kvashnina, S.M. Butorin, D. Cui, J. Vegelius, A. Puranen, R. Gens, P. Glatzel, J. Phys. Conf. Ser. 190 (2009) 012191.

[123] S.J. Oh, D.C. Cook, H.E. Townsend, Hyperfine Interact. 112 (1998) 59.

[124] M. Reffass, R. Sabot, C. Savall, M. Jeannin, J. Creus, Ph. Refait, Corros. Sci. 48 (2006) 709.

[125] C.T. Lee, M. Odziemkowski, D.W. Shoesmith, J. Electrochem. Soc. 153 (2006) B33.

[126] T. Ishikawa, Y. Kondo, A. Yasukawa, K. Kandori, Corros. Sci. 40 (1998) 1239.

[127] C. Ruby, A. Aissa, A. Géhin, J. Cortot, M. Abdelmoula, J.-M.R. Génin, C.R. Geosci. 338 (2006) 420.

[128] A. Puranen, M. Jonsson, R. Dähn, D. Cui, J. Nucl. Mater. 392 (2009) 519.

[129] A. Puranen, M. Jonsson, R. Dähn, D. Cui, J. Nucl. Mater. 406 (2010), 230.

[130] M. M. Hossain, E. Ekeroth, M. Jonsson, J. Nucl. Mater. 358 (2006) 202.

[131] O. Roth, H. Hasselberg, M. Jonsson, J. Nucl. Mater. 383 (2009) 231.